NASA CR-66169

COMPUTATION OF THE PRESSURE-TIME HISTORY OF A SONIC BOOM SHOCK WAVE ACTING ON A WINDOW GLASS IN A BUILDING

By Glen W. Zumwalt

Prepared under Contract
ANDREWS ASSOCIATES, INC.
Oklahoma City, Oklahoma

for

NATIONAL AERONAUTICS AND SPACE ADMINISTRATION

COMPUTATION OF THE

PRESSURE-TIME HISTORY OF A SONIC BOOM

SHOCK WAVE ACTING ON A WINDOW GLASS IN A BUILDING

By Glen W. Zumwalt

SUMMARY

Mathematical methods are presented for computing the pressure-time history of a sonic boom shock wave acting on any given exterior wall surface facing the shock wave. Also, for walls which are in the "shadow" of the shock wave or which receive reflected wave effects from nearby walls or corners, additional methods are presented. These methods are applied to a specific window location of a building wall at which it is believed the window glass was broken by a specific sonic boom from one test flight during the series of 1,253 sonic boom test flights at Oklahoma City in 1964.

The calculated pressure-time history acting on this window glass location, from this particular sonic boom, indicates that no abnormal or unusual pressure-time condition would have been produced. However, these calculations are based on several assumed atmospheric conditions and flight data values of which some are of doubtful validity.

INTRODUCTION

During the series of sonic boom test flights conducted in the Oklahoma City area during 1964, an 8' x 10' x 1/4" plate glass window in the store front of a single-story commercial building was broken coincidentally with the occurrence of one of the sonic booms. See Figure 1.

This particular sonic boom occurred at about 1:20 p.m. on Sunday, May 17, 1964 and was produced by an F-101 aircraft at 40,000 feet altitude on a scheduled steady-state course at a scheduled speed of Mach 1.4. Orientation and distance of aircraft course with respect to the building are shown in Figure 11.

Using this specific incident as an example, an attempt has been made to develop methods for predicting, or estimating, the pressure-time history acting on building walls in general when exposed to sonic boom shock waves. The pressure-time history is considered to include both bow and tail incident waves plus their respective reflected waves.

First considered is the time-of-passage of an incident wave and the time interval between incident and reflected waves for a wall facing the wave. This includes the following variables: aircraft velocity, altitude, and direction; wall angle, slope, and offset distance from the flight track. No wind effect is

included, but three atmospheric temperature models are used in the analysis.

The second analysis is concerned with N-wave diffraction and reflection around structures. The two-dimensional theory of Keller and Blank (Ref. 2) is adapted to produce a series of pressure perturbation expressions for multiple wave reflections.

The two analyses are applied to the location of the broken window in the example store front. Since the window location is under an overhanging roof of sufficient size to place it in the "shadow" of the shock wave, it provides almost all of the complications which can occur. Pressure-time histories are computed for the four corner points and the mid-point position of the window location. Since a two-dimensional analysis is used for the diffraction process, some idealization of the model was necessary.

A discussion is presented of a three-dimensional mesh-point computation technique which would permit treatment of three-dimensional, non-steady waves with arbitrary wall placement.

Purpose of this paper is intended to provide additional background information for further development of effective methods for predicting, investigating and evaluating possible sonic boom damage to window glass.

Figure 1 - Store front of the commercial building in which an 8' x 10' x 1/4" window glass was broken coincidentally with occurrence of a sonic boom. Third large pane from right is the location of broken window.

SYMBOLS FOR COMPUTATION OF SONIC BOOM WAVE PASSAGE TIMES ON A WALL

a	speed of sound ("acoustic velocity"), feet/second
D_{gv}	horizontal distance between the vertex of the sonic boom wave and its ground intersection point, g. (feet)
D_{pv}	horizontal distance between a wall point, P, and the vertex of the sonic boom wave, at the instant P is intersected by the incident wave. (feet)
H	height of the wall, feet
L	length of the wall, feet
m	coefficient of acoustic velocity variation with altitude, feet/second-feet
M	Mach number
S	projected distance of the wave from the flight path in the YZ plane; see Figure 3 . (feet)
t	time variable, seconds
T	time for a wave to pass a point after the aircraft passes the coordinate origin. (Subscripts indicate incident or reflected wave; second subscript indicates the point.) (seconds)
ΔT_{ir_p}	time interval between the passage of the incident and reflected waves at a point, P, on a wall. (seconds)
V	flight velocity, feet/second
X	coordinate axis, horizontal and along the flight track on the ground.
Y	coordinate axis, horizontal and perpendicular to the flight track.
Y_c	distance along the Y-axis to the nearest corner of the wall on the ground.
Z	coordinate axis, vertical.
β	Mach angle or incident wave angle measured from the horizontal.
θ	angle between the wall and the Y axis, measured clockwise from the Y axis in the horizontal plane.
τ	time at which a pressure disturbance wave was emitted. (seconds)

ϕ angle between the wall and the horizontal (X,Y) plane.

Subscripts:

c at point c, the lower corner of the wall which is the most "upstream" in the flight direction.

d at point d, the origin of the disturbance ray.

g at ground level point g, directly under the point P.

i incident wave.

p at point P on the wall.

r reflected wave.

t at the tropopause, or at the time a ray passed the tropopause plane.

v at the vertex of the shock cone.

SYMBOLS FOR DIFFRACTION AND REFLECTION OF SONIC BOOM WAVES BY CORNERS AND WALLS

a angle between wall and normal-to-wave

b angle between wall and normal-to-wave

c atmospheric velocity of sound, feet/second

C_1 first disturbance circle

C_2 second disturbance circle

C_3 third disturbance circle

C_4 fourth disturbance circle

H height of a wall, feet

n direction normal to a wall

p pressure perturbation $= \frac{P-P_o}{P_1-P_o}$ (dimensionless)

P pressure (psfa)

P_o atmospheric pressure (psfa)

P_1 pressure behind the incident wave (psfa)

r	transformed radial coordinate (see equation 4)
s	transformed time coordinate (see equation 4)
S	cross-sectional area of a ray tube, $feet^2$
t	time variable, seconds
W	transformed complex plane (see equation 11)
X	coordinate axis along the line of symmetry of a wedge or corner
X_1	coordinate axis along a horizontal wall
Y	coordinate axis perpendicular to X
Y_1	coordinate axis along a vertical wall
Z	complex variable (see equation 10)
λ	see equation 11
θ	angle variable; clockwise from the X-axis
ϕ	half-angle of a wall or corner; clockwise from X-axis
ρ	see equation 7
ψ	ray angle; clockwise from X-axis

Subscripts:

0	in undisturbed atmosphere
1	behind incident wave
2	behind reflected wave
i	incident wave
r	reflected wave

COMPUTATION OF SONIC BOOM WAVE PASSAGE TIMES ON A WALL

The purpose of this section is to develop a method for estimating the pressure-time history at any point on a building due to the passage of a sonic boom wave. To determine the time of passage of bow and tail waves and their reflections, the geometric relations between wall and wave must be known for a given aircraft altitude, direction, and speed. Three methods were attempted, ranging from a simple, highly idealized model to a more realistic, but complex, analysis.

Method I

An approximate method was developed to predict the time history of incident and reflected sonic boom waves on a plane wall. The simplifying assumptions made here were (a) that the speed of sound of the conical wave is constant and equal to that at ground level, and (b) that no wind effects are present. The wave then can be considered to be truly conical if the aircraft is in steady, level flight.

The coordinate axis system for an arbitrarily oriented plane wall is shown in Figure 2. The bow and tail waves are assumed to have been produced by an aircraft in steady, level flight at altitude Z_v, flying with a velocity V parallel to the X-axis. The horizontal distance of the effective vertex of the cone from a fixed origin "O", at the time the wave passes a given location on the wall, can be estimated. This distance is designated X_v. For a known geometry and forward speed of the aircraft, the time history of an incident wave on a plane wall can then be computed.

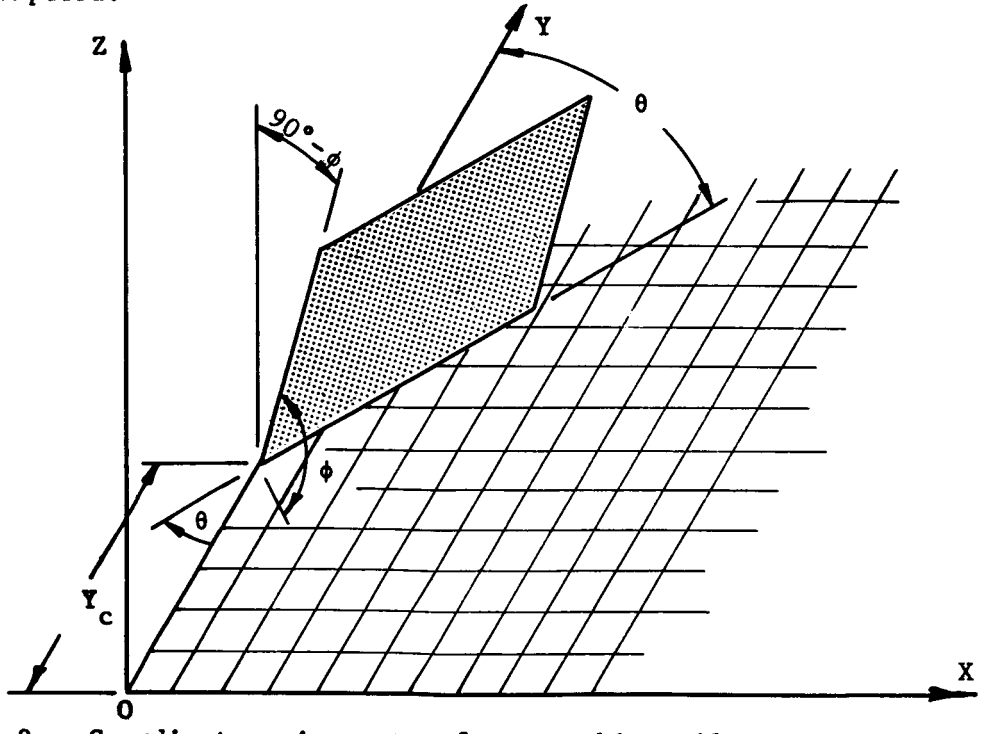

Figure 2 - Coordinate axis system for an arbitrarily oriented plane wall.

With reference to Figure 3 :

$$T_{i_p} = X_v/V \tag{1}$$

$$X_v = X_p + D_{pv} \tag{2}$$

$$X_p = (Y_p - Y_c) \text{ Tan } \theta + Z_p \frac{\text{Cot } \phi}{\text{Cos } \theta} \tag{3}$$

$$D_{pv} = \frac{\sqrt{Y_p^2 + (Z_v - Z_p)^2}}{\text{Tan } \beta} \tag{4}$$

The four equations can be combined to give the time the incident wave reaches point P on the wall:

$$T_{i_p} = \frac{1}{V} \left[(Y_p - Y_c) \text{ Tan } \theta + \frac{Z_p \text{ Cot } \phi}{\text{Cos } \theta} + \frac{\sqrt{Y_p^2 + (Z_v - Z_p)^2}}{\text{Tan } \beta} \right] \tag{5}$$

The time T_{i_p} is referenced to the passing of the aircraft over origin, O.

The time interval between the incident and reflected waves passing P is twice the time interval from P to the ground directly beneath:

$$\Delta T_{ir_p} = 2(T_{i_g} - T_{i_p}) \tag{6}$$

$$T_{i_g} = \frac{X_p + D_{gv}}{V} \tag{7}$$

$$D_{gv} = \frac{\sqrt{Y_p^2 + Z_v^2}}{\text{Tan } \beta} \tag{8}$$

Thus:

$$\Delta T_{ir_p} = \frac{2}{V} (D_{gv} - D_{pv}) \tag{9}$$

$$T_{ir_p} = \frac{2}{V} \text{ Cot } \beta \left[\sqrt{Y_p^2 + Z_v^2} - \sqrt{Y_p^2 + (Z_v - Z_p)^2} \right] \tag{10}$$

T_{i_p} and ΔT_{ir_p} values for a large number of points, P, on a wall will give a clear picture of the time-history of the incident and reflected waves for a wall which is struck by an undisturbed wave. This does not, of course, apply to wall which would be in the "shadow".

T_{ir_p} plays an important role in the structural response. From equation (10), it can be seen that this time interval increases with height of the wall point above ground level and decreases as the offset distance from the flight track increases.

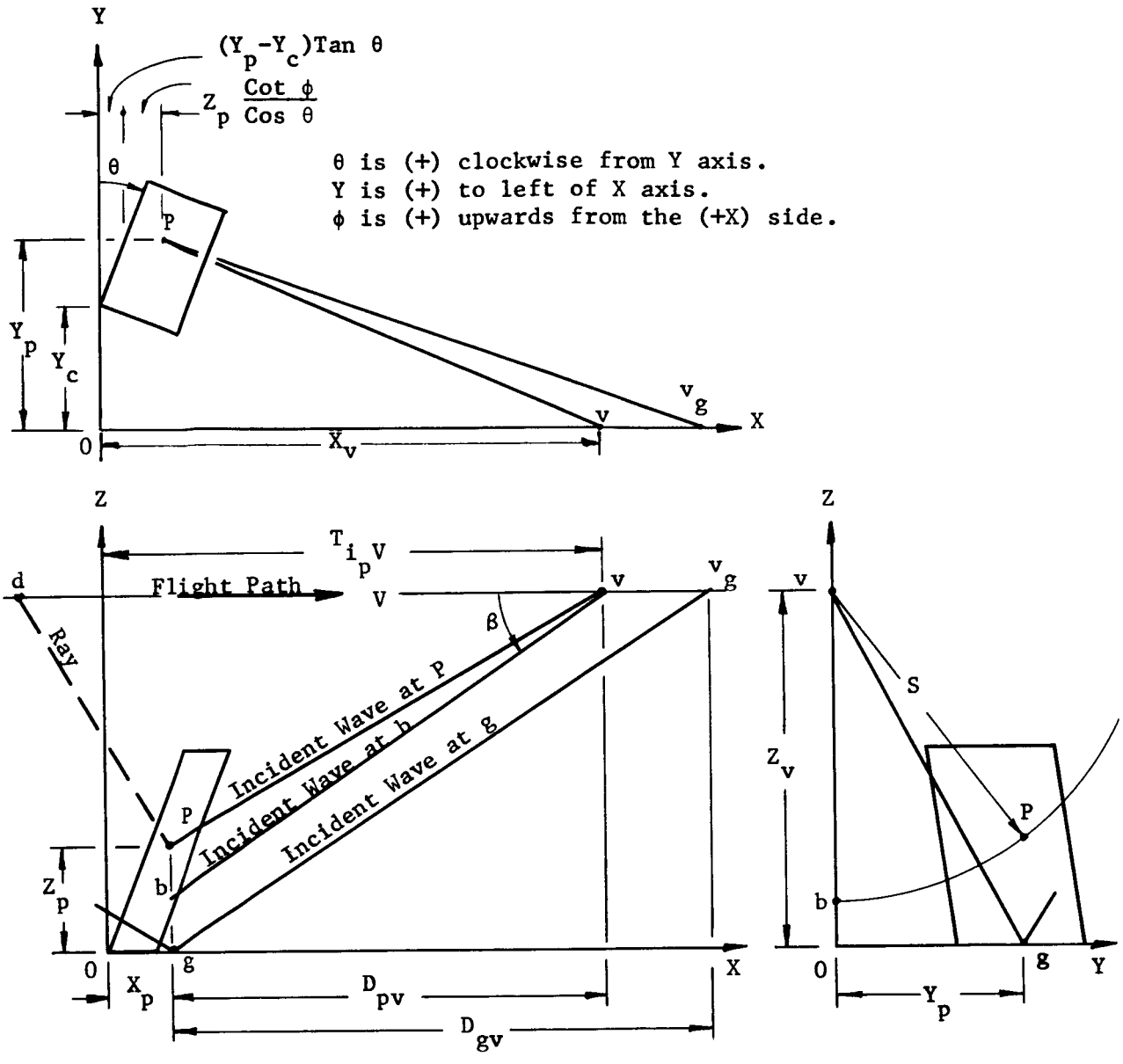

Figure 3 - Model for the analysis of a conical wave intersecting a plane, rectangular, sloping wall.

Method II

A more exact method, based on the ballistic wave analysis of Ref. 1 was developed. In this, the speed of sound was assumed to decrease linearly with altitude up to the tropopause (assumed as 36,000 feet), and constant at 972 ft/sec above the tropopause.

$$a = a_g - mZ \tag{11}$$

For a_g = 1116 ft/sec and m = 0.004 ft/sec-ft., the speed of sound is found to be

very near that of the standard atmosphere; see Figure 4 .

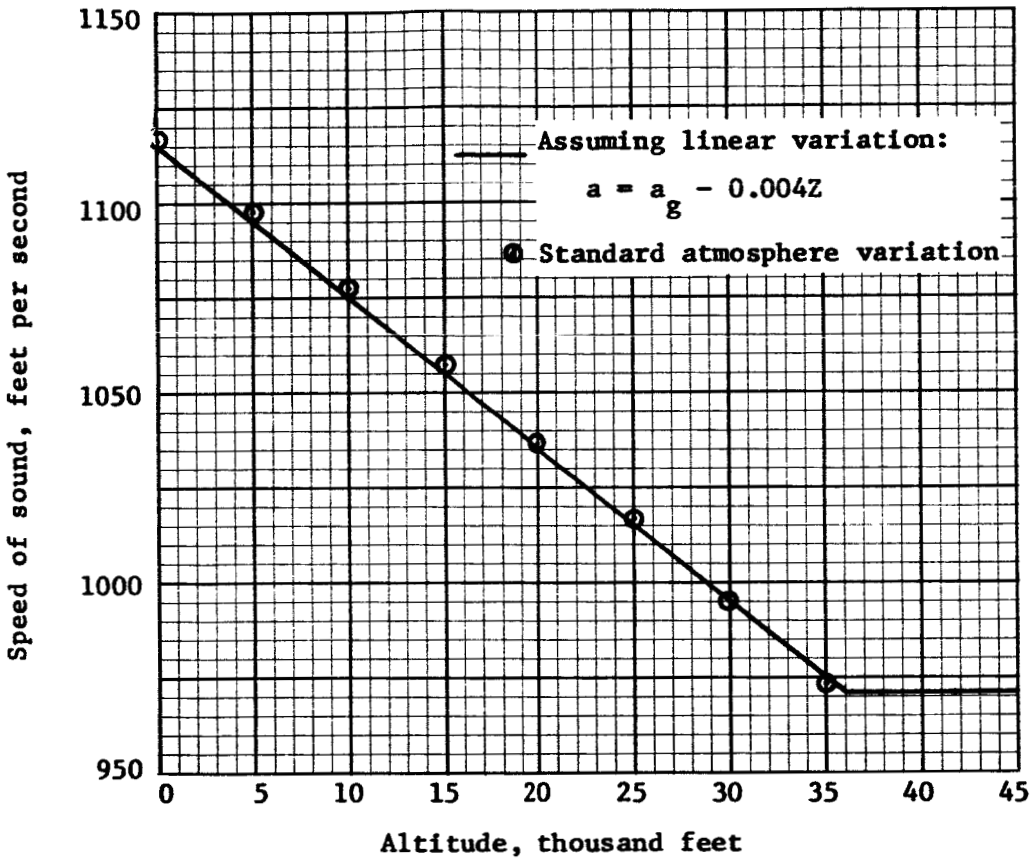

Figure 4 - Speed of sound vs. altitude.

Flight altitudes below the tropopause. - The shape of the wave fronts produced by a point disturbance is obtained by finding the system of surfaces which are orthogonal to rays from that point. By following that disturbance as it propagates from a point, along a given ray, it is possible to relate the shape of the wave fronts to the growth of these fronts. In an atmosphere in which the sonic speed decreases linearly with altitude, the disturbance front coordinates (X,Y,Z,) are given by:

$$(X-X_d)^2 = (Y-Y_d)^2 + \left[Z-Z_d + \frac{a_v}{m}(\text{Cosh } mt - 1)\right]^2 = \frac{a_v^2}{m^2}\,\text{Sinh}^2 mt \qquad (12)$$

The coordinates are as shown in Figure 3 , except that, for a non-constant-temperature atmosphere, the ray and wave lines are not straight. In equation (12), t is the time since the disturbance was initiated. Considering a fixed coordinate system as shown in Figure 3 , the disturbance origin, point d, becomes a function of time. Then at time t, the position of the wave front (X,Y,Z) emitted by the aircraft at an earlier time τ is given by:

$$(X-X_d)^2 + (Y-Y_d)^2 + \left\{Z-Z_d + \frac{a_v}{m}\left[\text{Cosh } m(t-\tau) - 1\right]\right\}^2 = \frac{a_v^2}{m^2}\,\text{Sinh}^2 m(t-\tau) \qquad (13)$$

where: $a_v = a_g - mZ_v$ and X_d, Y_d, and Z_d are functions of τ.

The envelope of this system of wave fronts is obtained by eliminating τ between equation (13) and its partial derivative with respect to Z. This differentiation gives:

$$-2\,(X-X_d)\,\dot{X}_d - 2\,(Y-Y_d)\,\dot{Y}_d - 2\left\{Z-Z_d + \frac{a_v}{m}\left[\text{Cosh } m\,(t-\tau)-1\right]\right\}$$
$$\left\{\dot{Z}_d+\dot{Z}_d\left[\text{Cosh } m\,(t-\tau) - 1\right] + a_v \text{ Sinh } m\,(t-\tau)\right\} =$$
$$-2\,\frac{a_v}{m}\,\text{Sinh } m\,(t-\tau)\left[a_v \text{ Cosh } m\,(t-\tau) + \dot{Z}_d \text{ Sinh } m\,(t-\tau)\right] \qquad (14)$$

For steady, level flight: $\dot{X}_d = V$ $\quad Y_d = 0$ (by coord. system)

$\dot{Y}_d = 0$ $\quad Z_d = \text{constant} = Z_v$

$\dot{Z}_d = 0$

Equation (14) then becomes

$$(X-X_d)\,V + \left\{Z-Z_v + \frac{a_v}{m}\left[\text{Cosh } m\,(t-\tau) - 1\right]\right\} \quad a_v \text{ Sinh } m\,(t-\tau) =$$
$$\frac{a_v^2}{m} \text{ Sinh } m\,(t-\tau) \text{ Cosh } m\,(t-\tau)$$

Simplifying:

$$X-X_d = -\frac{1}{M}\left(Z-Z_v - \frac{a_v}{m}\right) \text{Sinh } m\,(t-\tau) \qquad (15)$$

Combining (13) and (15):

$$\frac{1}{M^2}\left(Z-Z_v - \frac{a_v}{m}\right)^2 \text{Sinh}^2 m\,(t-\tau) + Y^2 + \left\{Z-Z_v + \frac{a_v}{m}\left[\text{Cosh } m\,(t-\tau) - 1\right]\right\}^2$$
$$= \frac{a_v^2}{m} \text{Sinh}^2 m\,(t-\tau) \qquad (16)$$

$$\frac{1}{M^2}\left(Z-Z_d - \frac{a_v}{m}\right)^2 \left[\text{Cosh}^2 m\,(t-\tau) - 1\right] + Y^2 + \left(Z-Z_d - \frac{a_v}{m}\right)^2 +$$

$$\frac{2a_v}{m}\left(Z-Z_d - \frac{a_v}{m}\right) \text{Cosh } m\,(t-\tau) + \frac{a_v^2}{m^2}\underbrace{\left[\text{Cosh}^2 m(t-\tau) - \text{Sinh}^2 m(t-\tau)\right]}_{=1} = 0 \qquad (16a)$$

$$\frac{1}{M^2}\left(Z-Z_v - \frac{a_v}{m}\right)^2 \text{Cosh}^2 m\,(t-\tau) + \frac{2a_v}{m}\left(Z-Z_v - \frac{a_v}{m}\right) \text{Cosh } m\,(t-\tau) +$$

$$Y^2 + \left(Z-Z_v - \frac{a_v}{m}\right)^2\left(1 - \frac{1}{M^2}\right) + \frac{a_v^2}{m^2} = 0 \qquad (16b)$$

By the quadratic formula:

$$\text{Cosh } m(t-\tau) = -\frac{M^2 a_v}{m}\left(Z-Z_v-\frac{a_v}{m}\right)^{-1} \pm \left\{\frac{4a_v^2}{m^2}\left(Z-Z_v-\frac{a_v}{m}\right)^2 - \frac{4}{M^2}\left(Z-Z_v-\frac{a_v}{m}\right)^2 \left[Y^2+\left(Z-Z_v-\frac{a_v}{m}\right)^2\left(1-\frac{1}{M^2}\right)+\frac{a_v^2}{m^2}\right]\right\}^{\frac{1}{2}} \left[\frac{2}{M^2}\left(Z-Z_v-\frac{a_v}{m}\right)^2\right]^{-1}$$

Simplifying:

$$\text{Cosh } m(t-\tau) = -\frac{M^2 a_v}{m(Z-Z_v-\frac{a_v}{m})}\left\{1 \pm \sqrt{1-\left(\frac{m}{a_v M}\right)^2\left[Y^2+\left(Z-Z_v-\frac{a_v}{m}\right)^2\left(1-\frac{1}{M^2}\right)+\frac{a_v^2}{m^2}\right]}\right\}$$

$$\text{Cosh } m(t-\tau) = \frac{M}{Z-Z_v-\frac{a_v}{m}}\left\{-\frac{Ma_v}{m} \pm \sqrt{\left(1-\frac{1}{M^2}\right)\left[\left(\frac{Ma_v}{m}\right)^2-\left(Z-Z_v-\frac{a_v}{m}\right)^2\right]-Y^2}\right\} \quad (17)$$

For $Z<Z_d$, the (+) sign applies before the radical in (17).

For given values of $Y = Y_p$, $Z = Z_p$, Z_v, and M, values of $(t-\tau)_p$ can be calculated by (17). The time-history of an incident wave is then given by:

$$T_{i_p} = \frac{1}{V}(X_p + D_{pv})$$

$$= \frac{1}{V}\left[(Y_p-Y_c)\text{ Tan }\theta + \frac{Z_p \text{Cot }\phi}{\text{Cos }\theta}\right] + (t-\tau)_p - \frac{(X_p-X_d)}{V} \quad (18)$$

Equation (15) will give (X_p-X_d) for the selected Z_d, with $(t-\tau)_p$ from (17).

For the time interval between incident and reflected waves,

$$T_{ir_p} = \frac{2}{V}(D_{gv} - D_{pv}). \quad (9)$$

For this linearly-varying speed of sound atmosphere,

$$D_{pv} = (t-\tau)_p V - (X_p-X_d) \text{ and } D_{gv} = (t-\tau)_g V - (X_g-X_{dg}) \quad (19) \text{ \& } (20)$$

The (X_g-X_{dg}) term can be obtained from (15); one can solve (17) for $(t-\tau)_g$ with $Y = Y_g = Y_p$ and $Z = Z_g = 0$.

Flight altitude above the tropopause. - An explicit solution is not possible for a given offset distance from the flight track. A method will be proposed, however, which will permit the computation of local positions and times of the wave.

For $Z_v \geq Z \geq Z_t$, where Z_t is the altitude of the tropopause (here assumed as 36,000 feet), the speed of sound will be assumed to be constant. The disturbance envelope at time t for a point disturbance emitted by the aircraft at time τ is a cone:

$$(X-X_d)^2 + (Y-Y_d)^2 + (Z-Z_d)^2 = a_d^2 (t-\tau)^2 \quad (21)$$

Differentiating (21) with respect to Z and recognizing that:

$$Y_d = 0 \qquad \dot{Y}_d = 0 \qquad \dot{a}_d = 0 \qquad a_d = a_v$$

$$Z_d = Z_v \qquad \dot{Z}_d = 0 \qquad \dot{X}_d = V$$

then

$$X - X_d = \frac{a_v(t-\tau)}{M} \,. \tag{22}$$

From equations (21) and (22):

$$Y^2 + (Z-Z_v)^2 = a_v^2\,(t-\tau)^2\,(1-1/M^2) \tag{23}$$

$$\left.\frac{\partial Y}{\partial Z}\right|_{ray} = \text{constant} = \frac{Y}{Z - Z_v}$$

At the tropopause, $Y = Y_t$ and $Z = Z_t = 36{,}000$ ft.

$$Y_t^2 + (Z_t - Z_v)^2 = a_v^2\,(t_t - \tau)^2\,(1-1/M^2) \tag{24}$$

$$\left.\frac{\partial Y}{\partial Z}\right|_{ray} = \frac{Y_t}{Z_t - Z_v} \tag{25}$$

For $Z_t \geq Z \geq 0$, the cone is "warped" by the temperature gradients and no exact analysis is available. For local wave positions and times, however, it is sufficient to consider only the ray which reaches the given point. If the ray at the tropopause plane is considered to be a point disturbance, the previously developed equations will describe its path. Then the location of the wave can be found as a function of time, working point-by-point with a ray-tracing procedure.

The equation for the disturbance envelope at time t of a point disturbance emitted at time t_t, at the tropopause plane, is:

$$\text{Cosh } m(t_p - t_t) = \frac{M}{\left(Z_p - Z_t - \frac{a_v}{m}\right)}\left\{-\frac{Ma_v}{m} + \sqrt{\left(1-\frac{1}{M^2}\right)\left[\left(\frac{Ma_v}{m}\right)^2 - \left(Z_p - Z_v - \frac{a_v}{m}\right)^2\right] - (Y_p - Y_t)}\right\} \tag{26}$$

Equation (26) can be solved as before, except that now the value of Y_t is not known. An iterative method must be used:

1. Assume a value of Y_t.
2. Calculate t_t and $\left.\frac{\partial Y}{\partial Z}\right|_{ray}$ at the tropopause by (24) and (25).

3. Assume that the slope will be constant for a selected ΔZ interval.

$$Y-Y_t = \frac{\partial Y}{\partial Z}\,\Delta Z \tag{27}$$

$$Z = Z_t - \Delta Z \tag{28}$$

4. Calculate $(t-t_t)$ using (26), and the techniques explained in the previous section. Calculate the new wave-slope as follows:

From equation (16), $\frac{\partial Y}{\partial Z}$ can be evaluated for the disturbance envelope which is everywhere perpendicular to the rays. Then differentiating (16) with respect to Z for a point disturbance at X_t, Y_t, Z_t:

$$\frac{2}{M^2}\left(Z-Z_t-\frac{a_t}{m}\right)\sinh^2 m(t-\tau)+2(Y-Y_t)\left.\frac{\partial Y}{\partial Z}\right|_{\substack{\text{dist.}\\ \text{envel.}}}+2\left(Z-Z_t-\frac{a_t}{m}\right)+2\,\frac{a_t}{m}\cosh m(t-\tau)=0 \tag{29}$$

Since $\left.\frac{\partial Y}{\partial Z}\right|_{\substack{\text{dist.}\\ \text{envel.}}}\left.\frac{\partial Y}{\partial Z}\right|_{\text{ray}} = -1$,

$$\left.\frac{\partial Y}{\partial Z}\right|_{\text{ray}} = (Y-Y_t)\left\{\left(Z-Z_t-\frac{a_t}{m}\right)\left[1+\frac{1}{M^2}\sinh^2 m(t-\tau)\right]+\frac{a_t}{m}\cosh m(t-\tau)\right\}^{-1}. \tag{30}$$

5. Repeat steps 3 and 4 until the desired Z value is obtained. If the computed Y does not give the desired location Y_p, select a new Y_t and repeat the five steps.

6. When the location has been obtained to sufficient accuracy, the T_{i_p} value is computed by (18) except now:

$$(t-\tau)_p = (t_t-\tau)_p + (t-t_t)_p$$

Find $(t_t-\tau)_p$ from (24) with the proper Y_t.

Find $(t-t_t)_p$ from (26).

$$(X_p-X_d) = (X_p-X_t) + (X_t-X_d)$$

Find (X_p-X_t) from (15) with X_t, Z_t, and t_t.

$$(X_t-X_d) = \frac{a_v}{M}(t_t-\tau)_p$$

7. For the g location, steps 1 through 5 must be performed again, with all p subscripts replaced by g. D_{gv} can now be found with $(t-\tau)_g$ and (X_g-X_{dg}) as was done for p in Step 6.

8. Compute ΔT_{ir_p} by (9).

Using an IBM 1620 computer and 500 ft. intervals for ΔZ, about 70 seconds was required for each complete iteration for a 50,000 foot altitude.

Method III

A third method was developed which attempted to reduce the computer time required by Method II without sacrificing too much accuracy. The simplifying assumption added was that $\frac{\partial Y}{\partial Z}$ of the ray was constant at the value of the flight altitude, while the linear variation of speed of sound with altitude below the tropopause was retained.

$$T_{i_p} = (X_p + D_{pv})\frac{1}{V} = \frac{1}{V}\left(X_p + \int_0^{S_p} \frac{dS}{\text{Tan } \beta}\right) \tag{31}$$

S is the projected distance of the wave from the flight path in the YZ plane; see Figure 3.

Flight altitudes below the tropopause. -

$$dS = (dY^2 + dZ^2) = -dZ\sqrt{1 + \left(\frac{dY}{dZ}\right)^2} \tag{32}$$

Assuming:

$\left.\frac{dY}{dZ}\right|_{ray}$ = constant = $\frac{Y-Y_v}{Z-Z_v}$, and Y_v is zero by the coordinate system,

$$dS = -dZ\sqrt{1 + \left(\frac{Y}{Z-Z_v}\right)^2} \tag{33}$$

For the linear sonic speed variation: $a = a_g - mZ$

$$da = -m\,dZ \quad \text{or} \quad Z = -\frac{da}{m} \tag{34}$$

$$\text{Tan } \beta = \frac{1}{\sqrt{M^2-1}} = \frac{a}{\sqrt{V^2-a^2}} \tag{35}$$

From equations (32) through (35), the time interval from aircraft overhead passage until wave passage at point P can be calculated:

$$T_{i_p} = \frac{1}{V}\left[X_p + \sqrt{1 + \left(\frac{Y_p}{Z_p-Z_v}\right)^2}\int_{a_v}^{a_p} \sqrt{\frac{v^2-a^2}{ma}}\,da\right]$$

$$T_{i_p} = \frac{1}{V}\left[(Y_p-Y_c)\,\text{Tan } \theta + \frac{Z_p \text{ Cot } \phi}{\text{Cos } \theta}\right] + \frac{1}{mV}\sqrt{1 + \left(\frac{Y_p}{Z_p-Z_v}\right)^2}\left[\sqrt{V^2-a_p^2} - \sqrt{V^2-a_v^2} + V \ln\left(\frac{V + \sqrt{V^2-a_v^2}}{V + \sqrt{V^2-a_p^2}}\,\frac{a_p}{a_v}\right)\right] \tag{36}$$

$$\Delta T_{ir_p} = \frac{2}{V}(D_{gv} - D_{pv}) \tag{9}$$

Where:

$$D_{gv} = \frac{1}{m}\sqrt{1 + \left(\frac{Y_p}{Z_v}\right)^2}\left[\sqrt{V^2-a_g^2} - \sqrt{V^2-a_v^2} + V \ln\left(\frac{V + \sqrt{V^2-a_v^2}}{V + \sqrt{V^2-a_g^2}}\,\frac{a_g}{a_v}\right)\right] \tag{37}$$

and:

$$D_{pv} = \frac{1}{m}\sqrt{1+\left(\frac{Y_p}{Z_p-Z_v}\right)^2}\left[\sqrt{V^2-a_p^2} - \sqrt{V^2-a_v^2} + V\ln\left(\frac{V+\sqrt{V^2-a_v^2}}{V+\sqrt{V^2-a_p^2}}\,\frac{a_p}{a_v}\right)\right] \quad (38)$$

From (36), (37), and (38), T_{i_p} and ΔT_{ir_p} can be computed.

Flight altitudes above the tropopause. -

$$T_{i_p} = \frac{1}{V}\left[X_p + \int_0^{S_p}\frac{dS}{\text{Tan }\beta}\right] = \frac{1}{V}\left[X_p + \int_0^{S_t}\frac{dS}{\text{Tan }\beta} + \int_{S_t}^{S_p}\frac{dS}{\text{Tan }\beta}\right] \quad (39)$$

$$\int_0^{S_t}\frac{dS}{\text{Tan }\beta} = \int_{Z_v}^{Z_t}\frac{-dZ}{\text{Tan }\beta_t}\sqrt{1+\left(\frac{Y}{Z-Z_v}\right)^2} = \frac{Z_v-Z_t}{\text{Tan }\beta_t}\sqrt{1+\left(\frac{Y_t}{Z_t-Z_v}\right)^2}$$

$$= \frac{Z_v-Z_t}{a_v}\sqrt{V^2-a_v^2}\sqrt{1+\left(\frac{Y_t}{Z_t-Z_v}\right)^2} \quad (40)$$

By assumption: $\frac{Y_t}{Z_t-Z_v} = \frac{Y_p}{Z_p-Z_v}$

$$\int_{S_t}^{S_p}\frac{dS}{\text{Tan }\beta} = \frac{1}{m}\sqrt{1+\left(\frac{Y_p}{Z_p-Z_v}\right)^2}\left[\sqrt{V^2-a_p^2} - \sqrt{V^2-a_v^2} + V\ln\left(\frac{V+\sqrt{V^2-a_v^2}}{V+\sqrt{V^2-a_p^2}}\,\frac{a_p}{a_v}\right)\right] \quad (41)$$

(as in equation (36))

Then (39) becomes:

$$T_{i_p} = \frac{1}{V}\left[(Y_p-Y_c)\,\text{Tan }\theta + Z_p\,\frac{\text{Cot }\phi}{\text{Cos }\theta}\right] + \frac{1}{V}\sqrt{1+\left(\frac{Y_p}{Z_p-Z_v}\right)^2}\left[\sqrt{M^2-1}\,(Z_v-Z_t) + \frac{1}{m}\left(\sqrt{V^2-a_p^2} - \sqrt{V^2-a_v^2}\right) + \frac{V}{m}\ln\left(\frac{V+\sqrt{V^2-a_v^2}}{V+\sqrt{V^2-a_p^2}}\,\frac{a_p}{a_v}\right)\right] \quad (42)$$

$$T_{i_g} = \frac{1}{V}\left[(Y_p-Y_c)\,\text{Tan }\theta + Z_p\,\frac{\text{Cot }\phi}{\text{Cos }\theta}\right] + \frac{1}{V}\sqrt{1+\left(\frac{Y_p}{Z_v}\right)^2}\left[\sqrt{M^2-1}\,(Z_v-Z_t) + \frac{1}{m}\left(\sqrt{V^2-a_g^2} - \sqrt{V^2-a_v^2}\right) + \frac{V}{m}\ln\left(\frac{V+\sqrt{V^2-a_v^2}}{V+\sqrt{V^2-a_g^2}}\,\frac{a_g}{a_v}\right)\right] \quad (43)$$

These values can be used to obtain the incident-to-reflected time interval:

$$\Delta T_{ir_p} = 2 (T_{i_g} - T_{i_p})$$

Method III is much more straightforward to compute than Method II, but the assumption of constant ray angle places its accuracy in doubt. Therefore, a number of typical cases were computed by the three methods to provide a comparison of the results.

Computed results by the three methods. - To compare the three methods, computations were performed for a position on a vertical wall 100 feet above ground level. The ground level was taken as being at sea level, and flight altitudes of 70,000, 36,000, and 20,000 feet were used. For flight Mach numbers of 1.5, 2.0, and 3.0 and offset distances, Y_p from 0 to 70,000 feet, the three methods gave values of incident wave arrival time, T_{i_p}*, and time interval between incident and reflected waves, ΔT_{ir_p}. Figures 5 , 6 , and 7 show T_{i_p} and Figures 8 , 9 , and 10 show ΔT_{ir_p}.

For small offset distances, the three methods give almost identical results. The differences are greatest at low Mach numbers and large Y_p values. Method I, the conical wave analysis, gives the poorest accuracy, if it is assumed that Method II is the most exact of the three. Method III, which is considerably easier to calculate, appears to be nearly equivalent to Method II, and is the one recommended for use.

It should be emphasized that no accounting for wind has been taken, and that a linear variation of acoustic velocity with altitude was assumed.

Converting wave time-histories into wave geometry. - For the Kinney Shoe Store, the predicted position of the wave relative to the building was needed, as well as the time-of-passage of the waves at specific locations. The geometry can be found from the time values as described below.

To determine the angle between wave and wall in a horizontal plane, compute the T_i values for two points on the wall in the same horizontal plane, as for example, the lower corners of a building. If the distance between these points is L, and the point having the smaller Y coordinate is point 1 and the larger is point 2, the XY plane is shown in the following sketch.

---

* For these curves, the time reference for T_{i_p} is the time the wave passes the coordinate origin.

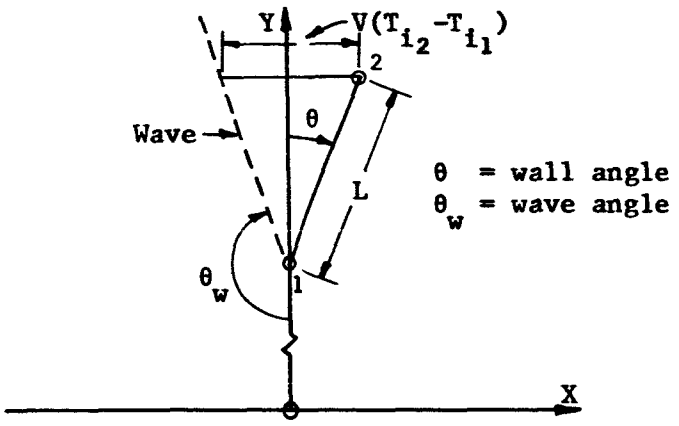

It can be shown, by use of the law of sines, that the wave angle is

$$\text{Tan } \theta_w = \text{Tan } \theta - (\text{Sec } \theta) \frac{V}{L} (T_{i_2} - T_{i_1})$$

Similarly, two points can be chosen on a vertical line, such as the upper and lower points of the corner of a building, with the upper designated 3 and the lower 4. Then, a vertical plane perpendicular to the wave line found above (i.e., at an angle $\theta_w + 90°$ from the Y axis) is as shown.

Then, for a wall height H,

$$\frac{1}{\text{Sin } \phi_w} - \text{Sin } \phi_w = \frac{a}{H} (T_{i_4} - T_{i_3})$$

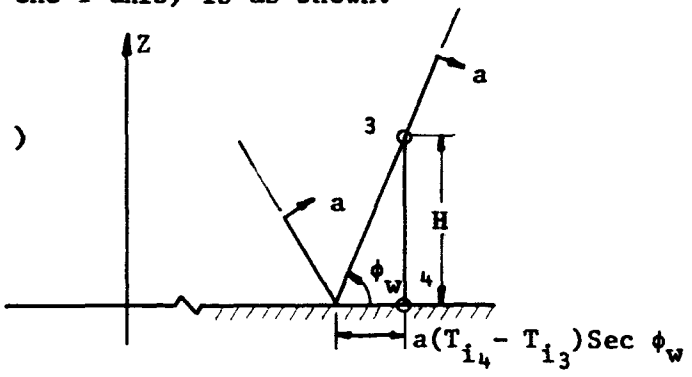

These relations were applied to the Kinney Shoe Store conditions. For this, the geometry is shown in Figure 11, and L= 70 ft., H= 12.75 ft. Values of $(T_{i_2} - T_{i_1})$ and $(T_{i_4} - T_{i_3})$ were found to be 0.0031 and 0.0014 seconds, respectively. From this, θ_w is found to be 26.8°, making the angle between wall and wave $(\theta - \theta_w) = 3.2°$. The wave elevation angle is $\phi_w = 70.1°$. The resulting wave-building relationship is shown in Figure 12 and some wave-time positions are depicted in Figure 13.

From test data for the F-101 aircraft at the flight Mach number, altitude, and the Y distance, the bow-to-tail wave time interval was estimated to be 0.135 seconds. Upon computing the incident-to-reflected wave time interval, ΔT_{ir}, for 6.0 and 12.75 feet heights, the pressure histories shown in Figure 14 could be predicted.

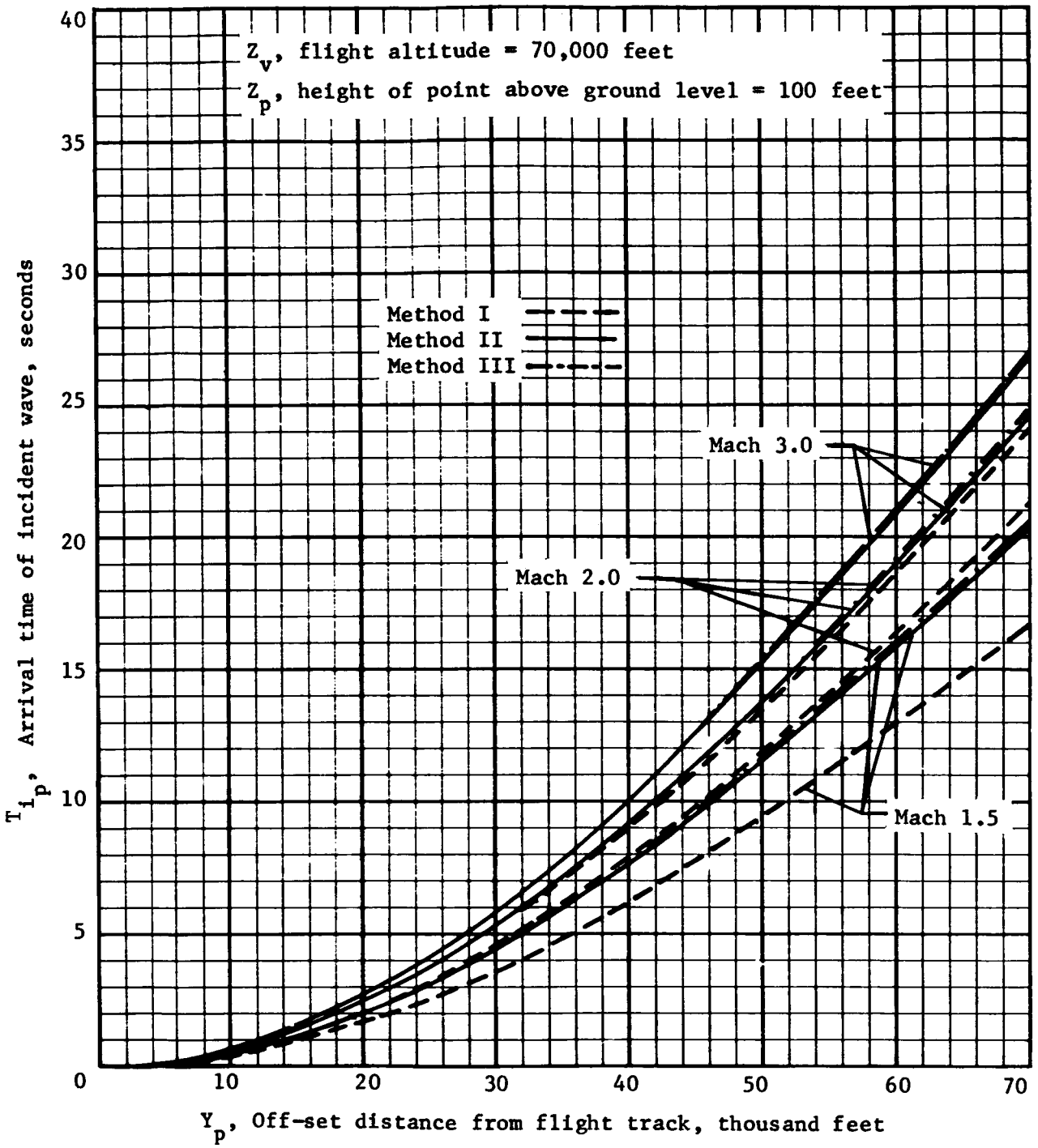

Figure 5 - Comparison of incident wave arrival time by three methods for flight altitude of 70,000 feet.

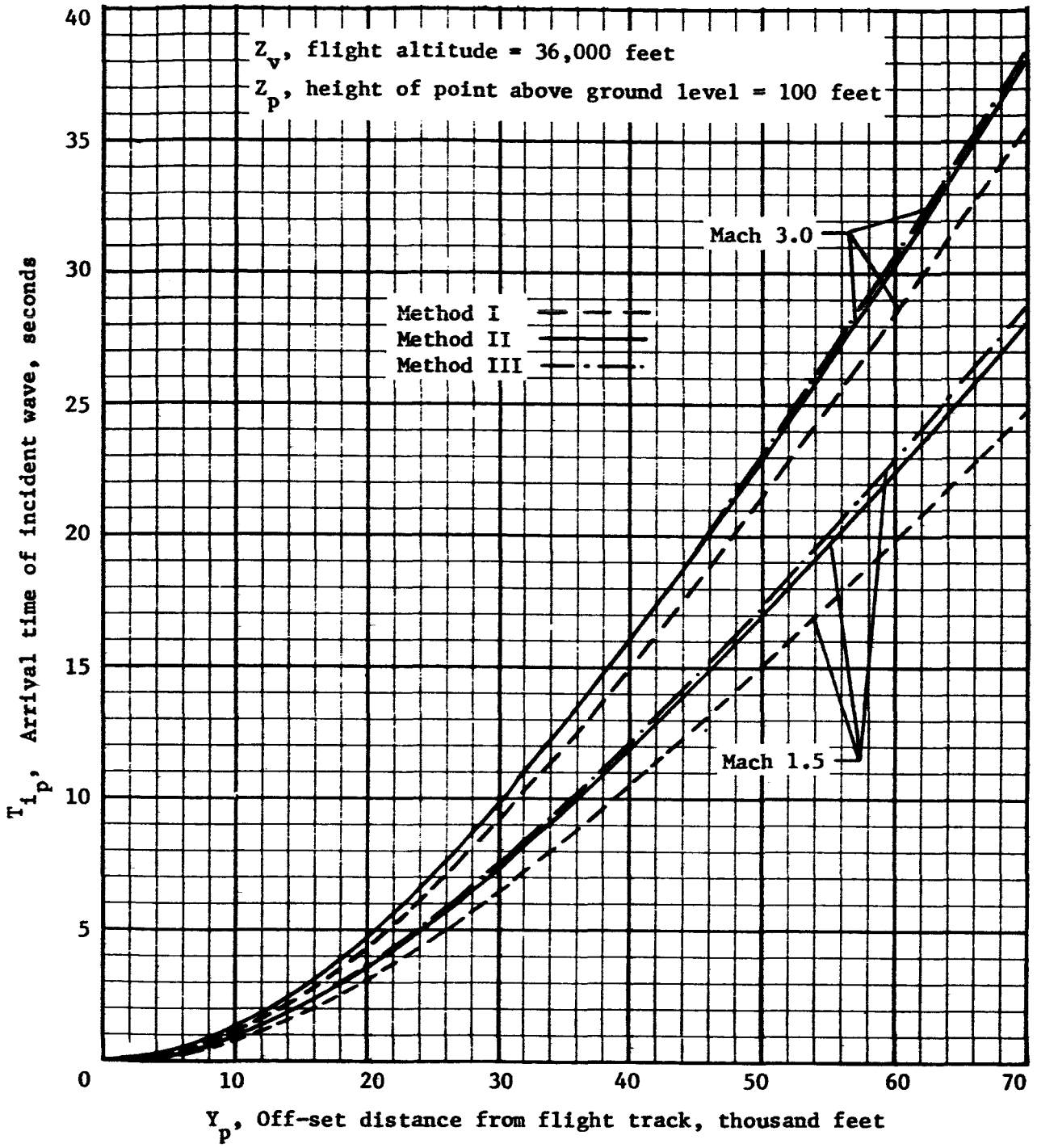

Figure 6 - Comparison of incident wave arrival time by three methods for flight altitude of 36,000 feet.

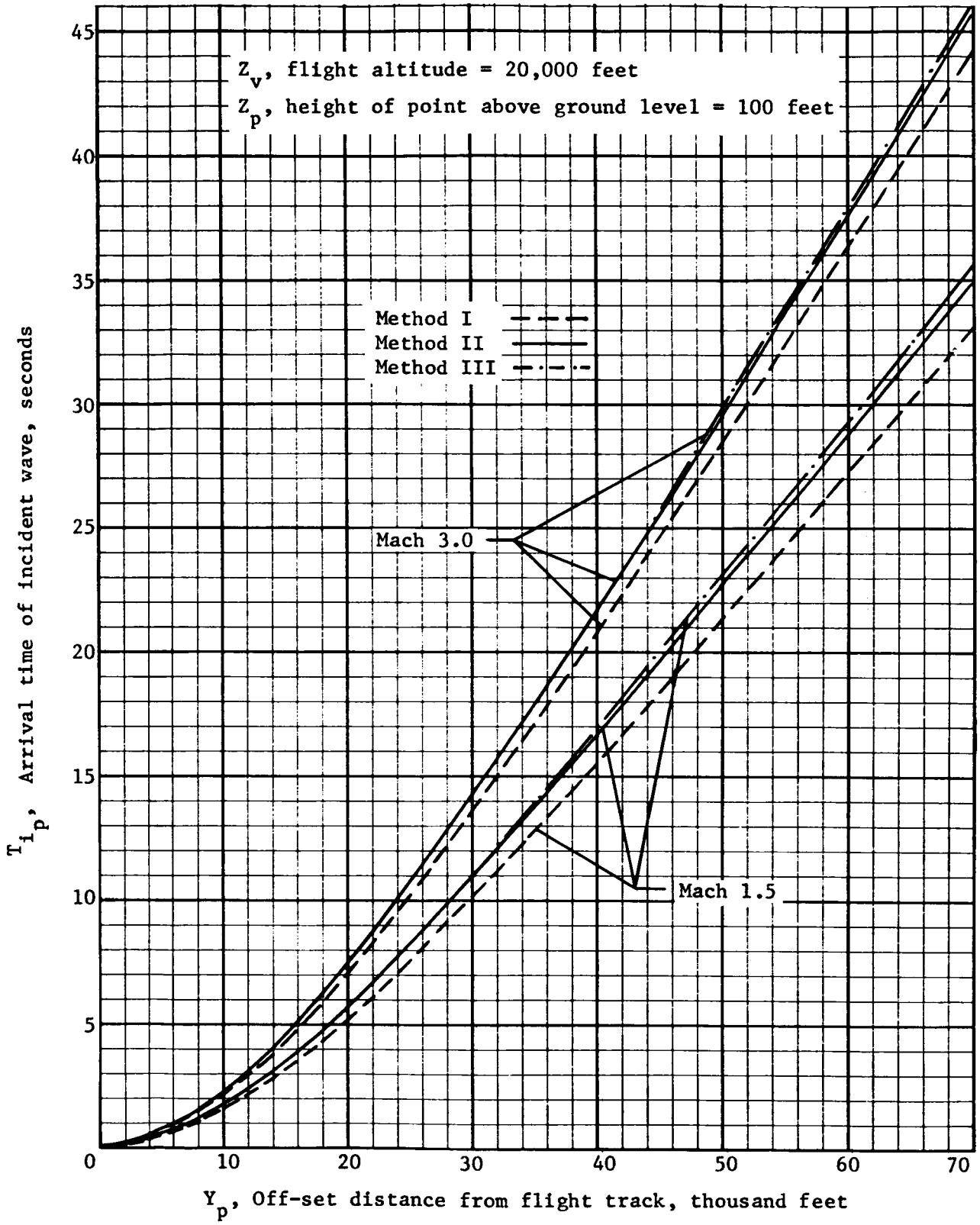

Figure 7 - Comparison of incident wave arrival time by three methods for flight altitude of 20,000 feet.

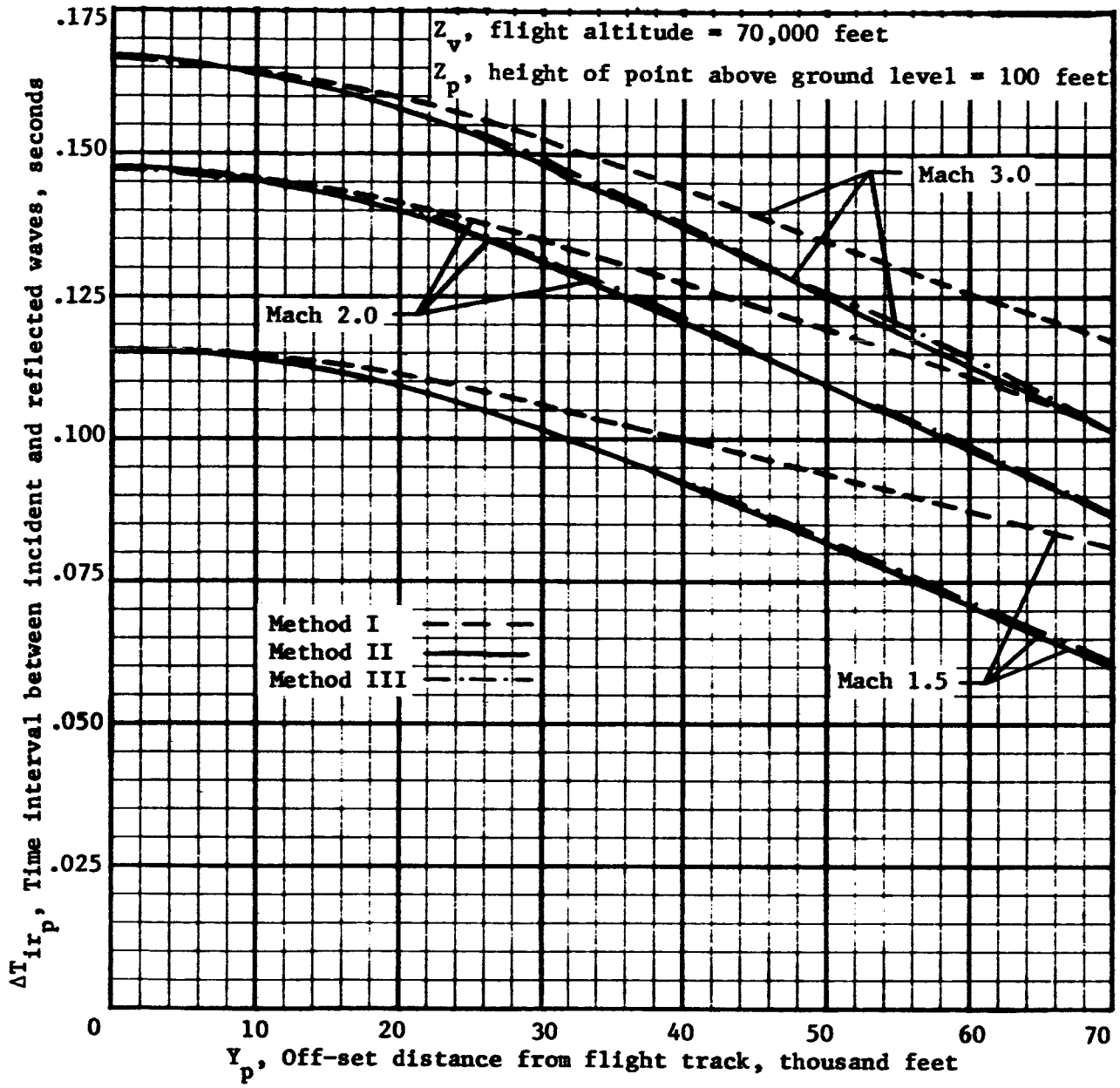

Figure 8 - Comparison of the time intervals between incident and reflected waves computed by three methods for flight altitude of 70,000 feet.

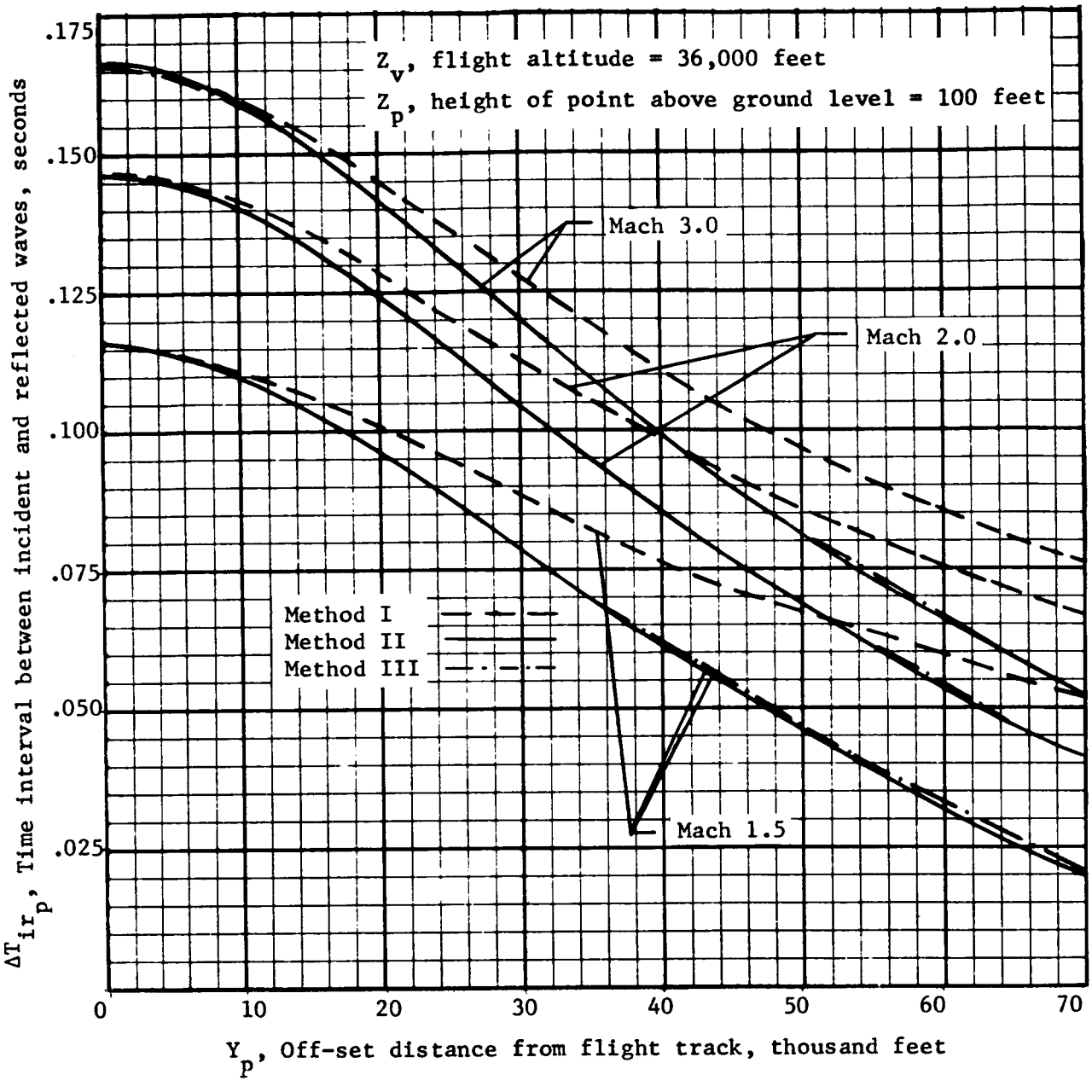

Figure 9 - Comparison of the time intervals between incident and reflected waves computed by three methods for flight altitude of 36,000 feet.

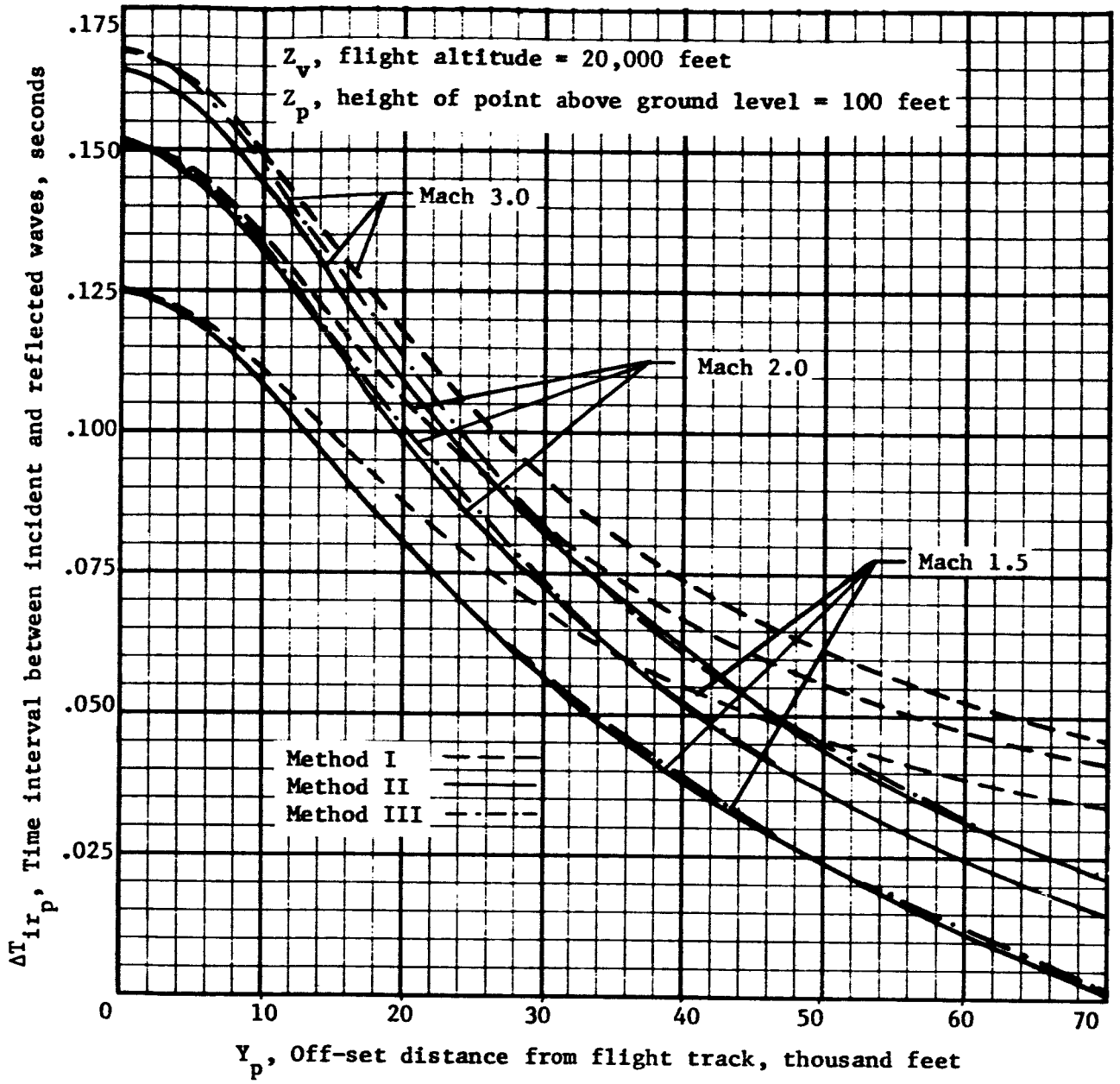

Figure 10 - Comparison of the time intervals between incident and reflected waves computed by three methods for flight altitude of 20,000 feet.

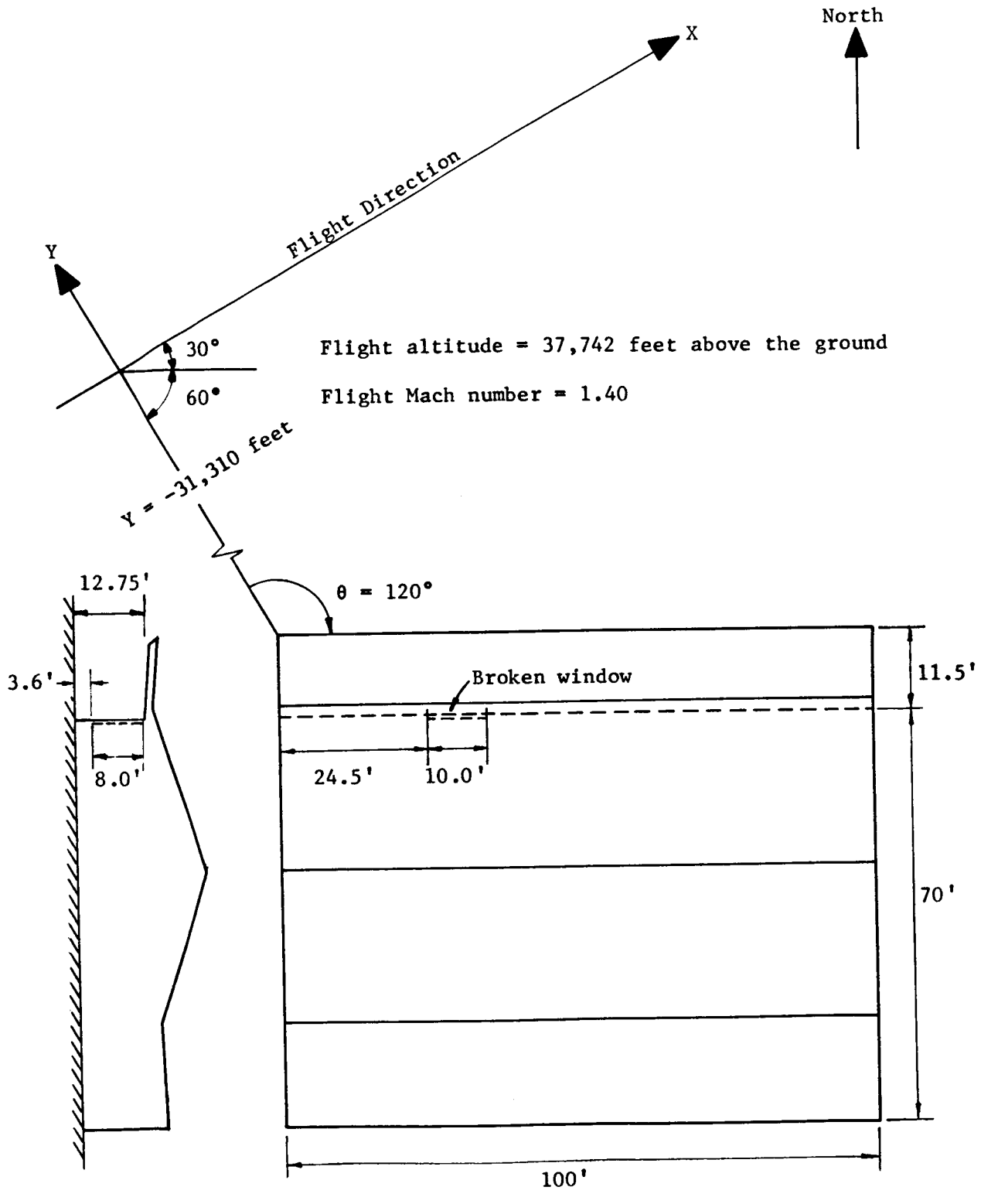

Figure 11 - Geometry used in the wave-history computations for the Kinney Shoe Store.

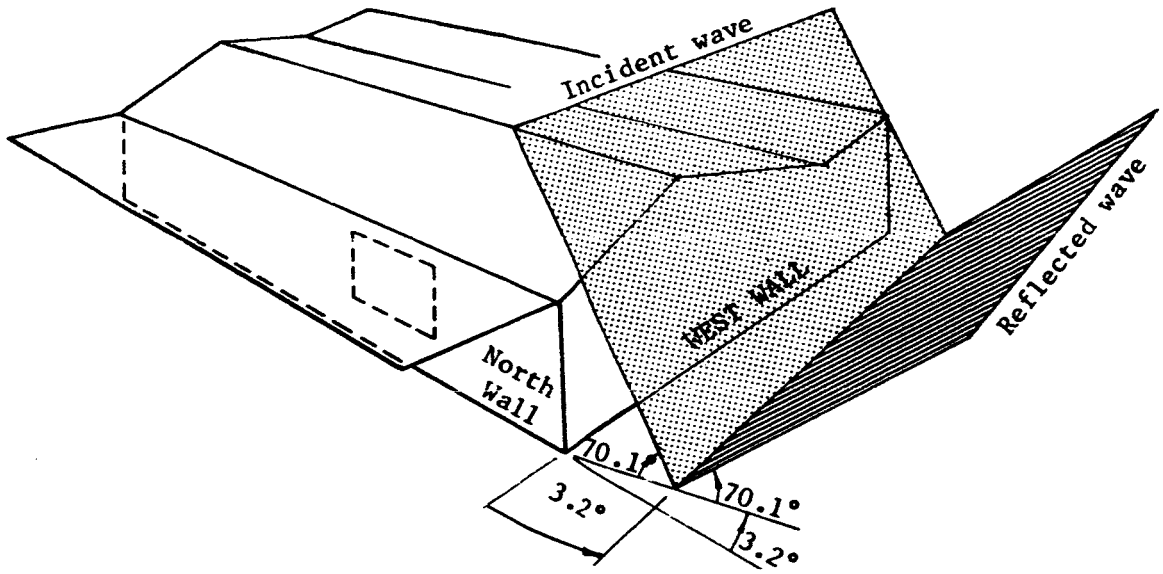

Figure 12 - Geometric relationship of building and wave.

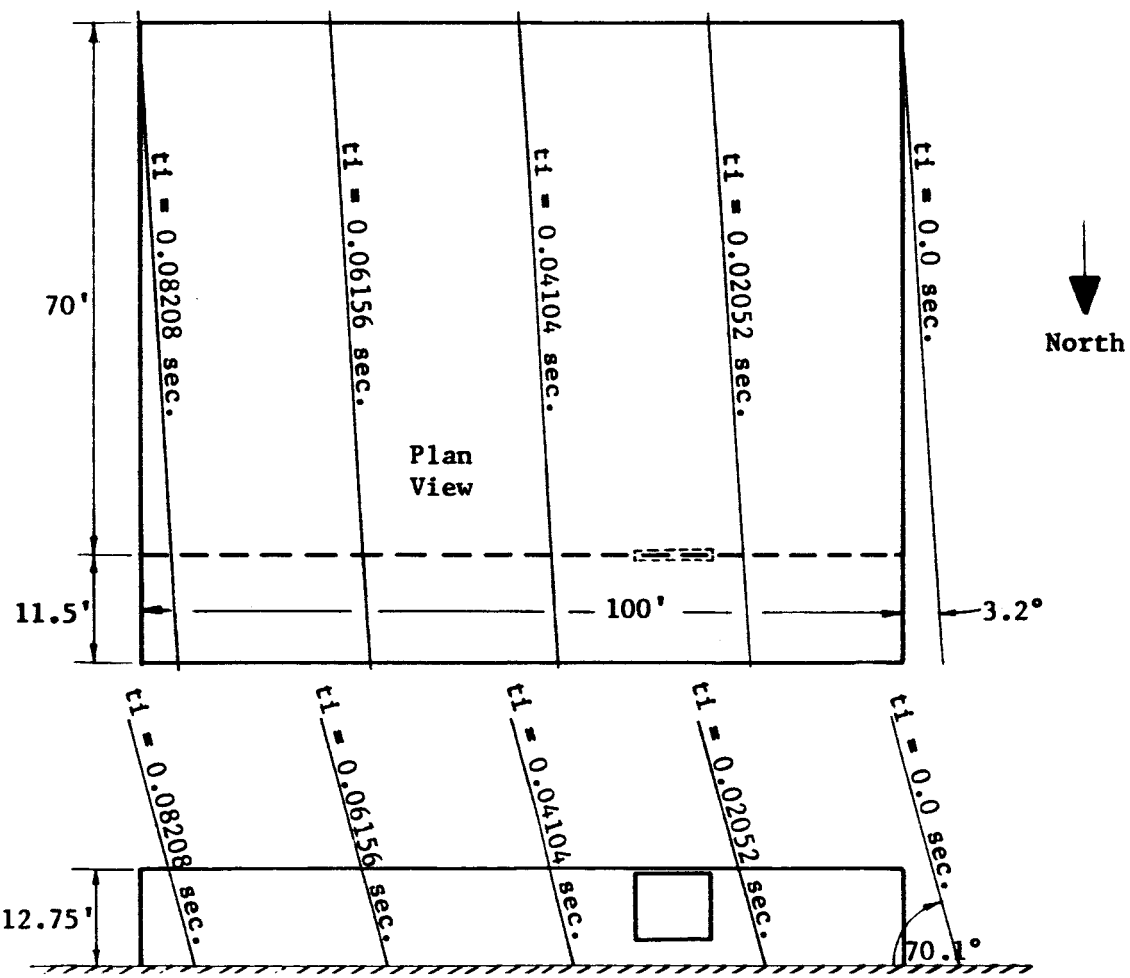

Figure 13 - Wave-history of incident wave of sonic boom wave on Kinney Shoe Store.

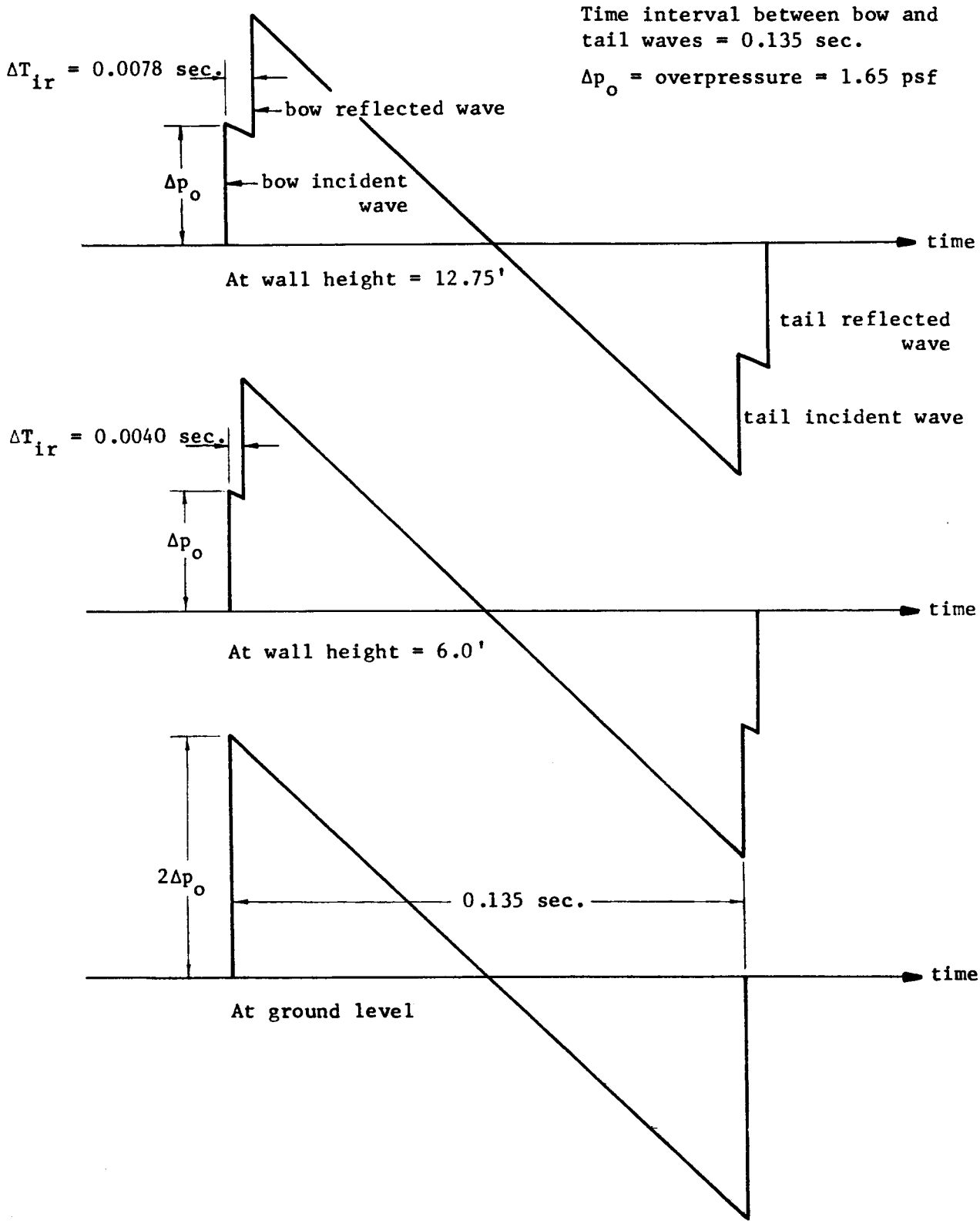

Figure 14 - Sonic boom pressure histories on the Kinney Shoe Store west wall.

DIFFRACTION AND REFLECTION OF SONIC BOOM WAVES BY CORNERS AND WALLS

The preceeding section presented a method for predicting the wave histories of walls which were hit directly by a sonic boom wave. For walls which are in the "shadow" or which receive the reflected effects of nearby walls or corners, a further development is required. In particular, the broken window in the Kinney Shoe Store was both in the shadow region and beneath an overhanging canopy. In the time interval between bow and tail shock, there was sufficient time for nearly twenty wave reflections between the ground and the overhanging roof. It is obviously hopeless to attempt to predict the pressure history on the window without reliance on a computer programmed to include both wave input and proper boundary conditions. Such a technique will be outlined below.

Sonic booms are considered to act as acoustic waves, or plane weak pulses, since they are very weak shock waves. In Reference 2 , the diffraction and reflection of an incident plane pulse by wedges and corners has been treated and explicit, closed-form expressions have been obtained in terms of elementary functions. For this geometry the solution is "conical" and independent of "radial" distance in the XYt space. This allows separation into appropriate coordinates, as in Busemann's conical flow method widely used in supersonic aerodynamics. The propagation of plane discontinuities has been investigated by Luneberg, Reference 3 , in electromagnetic theory, and by Keller, Reference 4, in acoustics. It is found that in both cases the discontinuity surface satisifes a first order differential equation, the eiconal equation, in a homogeneous media, and that the magnitude of the discontinuity varies in a simple manner. Making use of these results, in Reference 2 , the initial-boundary value problem has been converted into a characteristic-boundary value problem in XYt space and then the conical flow method has been used to obtain the solution.

A solution is sought to the acoustic wave equation in a two-dimensional geometry.

$$p = \frac{P - P_0}{P_1 - P_0}$$

$$p_{xx} + p_{yy} = \frac{1}{c^2} p_{tt} \qquad (1)$$

in the region $\phi \leq \theta \leq 2\pi - \phi$

where θ is the polar angle,

$$\theta = \arctan Y/X.$$

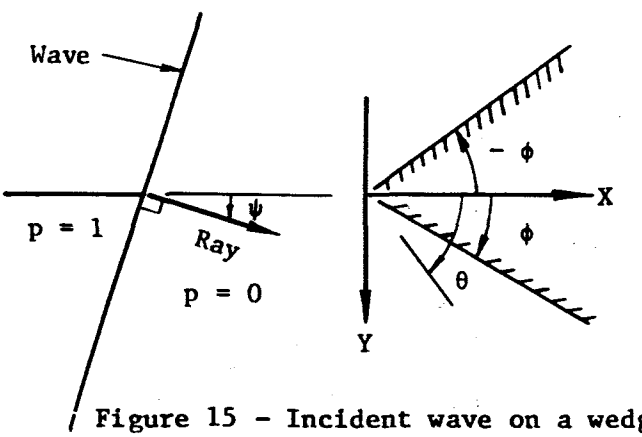

Figure 15 - Incident wave on a wedge.

By definition, the half-planes at $\theta = \pm \phi$ form a wedge or corner, depending on whether ϕ is less or greater than 90°.

The solution to be considered will have jump discontinuities on certain moving surfaces representing the shock wave, say $r(X,Y) = ct$. We require that r satisfy the eiconal equation.

$$\left(\frac{\partial r}{\partial X}\right)^2 + \left(\frac{\partial r}{\partial Y}\right)^2 = 1 \tag{2}$$

This implies that the surface can be constructed by Huygen's principle, that it moves with velocity c along its normal, and that it is reflected from the wall in accordance to the simple reflection law. A further assumption is that the reflected discontinuity value is twice the incident, following the rigid wall assumption $\frac{\partial p}{\partial n} = 0$.

The orthogonal trajectories of a family of discontinuity surfaces S(t) are straight lines called rays. The set of rays through a small closed curve on a discontinuity surface $S(t_o)$ is called a "tube". Denote the area of the tube at $S(t_o)$ by dS_o and the area of the tube at S(t) by dS. Also, the pressure discontinuities at $S(t_o)$ and S(t) are p_o and p, respectively. Then, for plane geometry, the magnitudes of the discontinuities must vary inversely as $\sqrt{dS}$:

$$\operatorname{Lim}_{dS \to 0} \left(\frac{dS}{dS_o}\right)^{\frac{1}{2}} = \frac{p_o}{p} \tag{3}$$

Equation (3) permits p to be computed from p_o on the same ray, once the discontinuity surfaces are known.

Referring to Figure 15, the ray direction is normal to the discontinuity plane and is positive in the direction of motion. The angle between the ray direction and the X axis is ψ, and it is always positive.

It follows from (2) that a plane discontinuity surface moves parallel to itself with velocity c along its normal and from (3) that a pressure jump, p=1, across the wave front does not change. This situation continues until the wave reaches the wedge. Then reflected and diffracted discontinuity surfaces may originate. These surfaces can be obtained from the configuration at the instant of contact. Then the incident plane progresses parallel to itself, and one (for $\psi \geq \phi$) or two (for $\psi \leq \phi$) reflected plane discontinuity surfaces plus a circular cylindrical surface with the wedge as its axis are produced: See Figures 16 and 17 .

The pressure jump across the original plane is unchanged and the jump across the reflected plane wave is equal to that of the incident, making p=2. The pressure jump across the cylindrical wave is zero, however, since all rays reaching it come from the axis where $dS_o = 0$. Thus, p is not discontinuous across the cylinder. The value of p everywhere outside the cylinder is known (either 0, 1, or 2). Since $\frac{\partial p}{\partial n} = 0$ on the wedge and p is continuous across the circular arc, the values on the boundary are known. From these values it is possible to determine the p values within the cylinder.

The wave patterns are self-similar with respect to time, and so can be presented in X/ct and Y/ct coordinates, as in Figures 16 and 17 . Solutions are to be sought inside the circle along radial lines from the origin. A set of special polar coordinates in XYt space will be used for this solution, which follows the method of Keller and Blank; Reference 2 .

$$r = \left[c^2t^2 - (X^2 + Y^2)\right]^{\frac{1}{2}}$$
$$s = ct/r \qquad (4)$$
$$\theta = \mathrm{Tan}^{-1} Y/X$$

The boundary of the circle is given by r = 0 and s = ∞, and equation (1) becomes

$$(r^2 p_r)_r + \left[(1-s^2)p_s\right]_s + \frac{1}{1-s^2} P_{\theta\theta} = 0 \qquad (5)$$

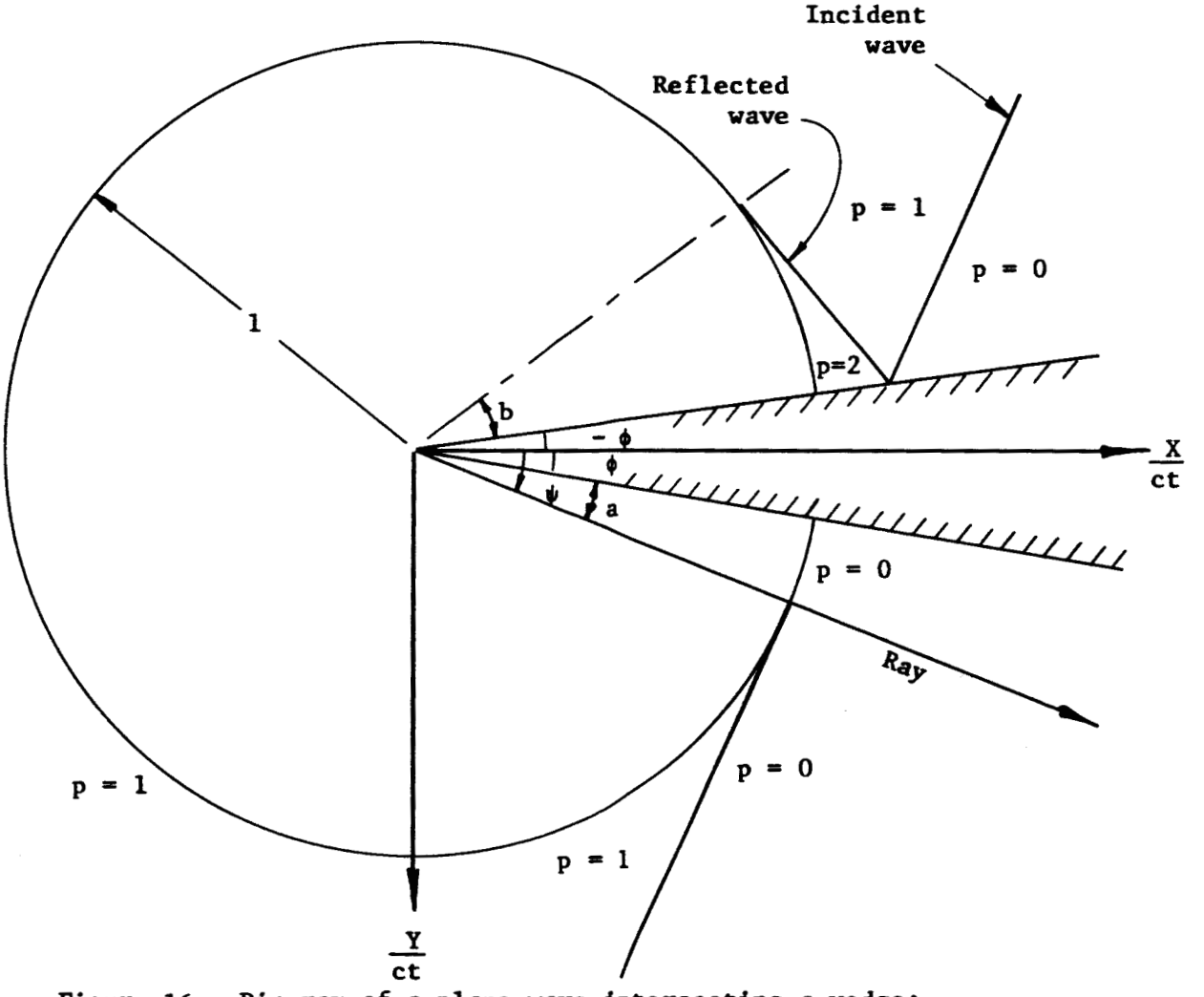

Figure 16 - Diagram of a plane wave intersecting a wedge; One reflected wave.($\psi > \phi$)

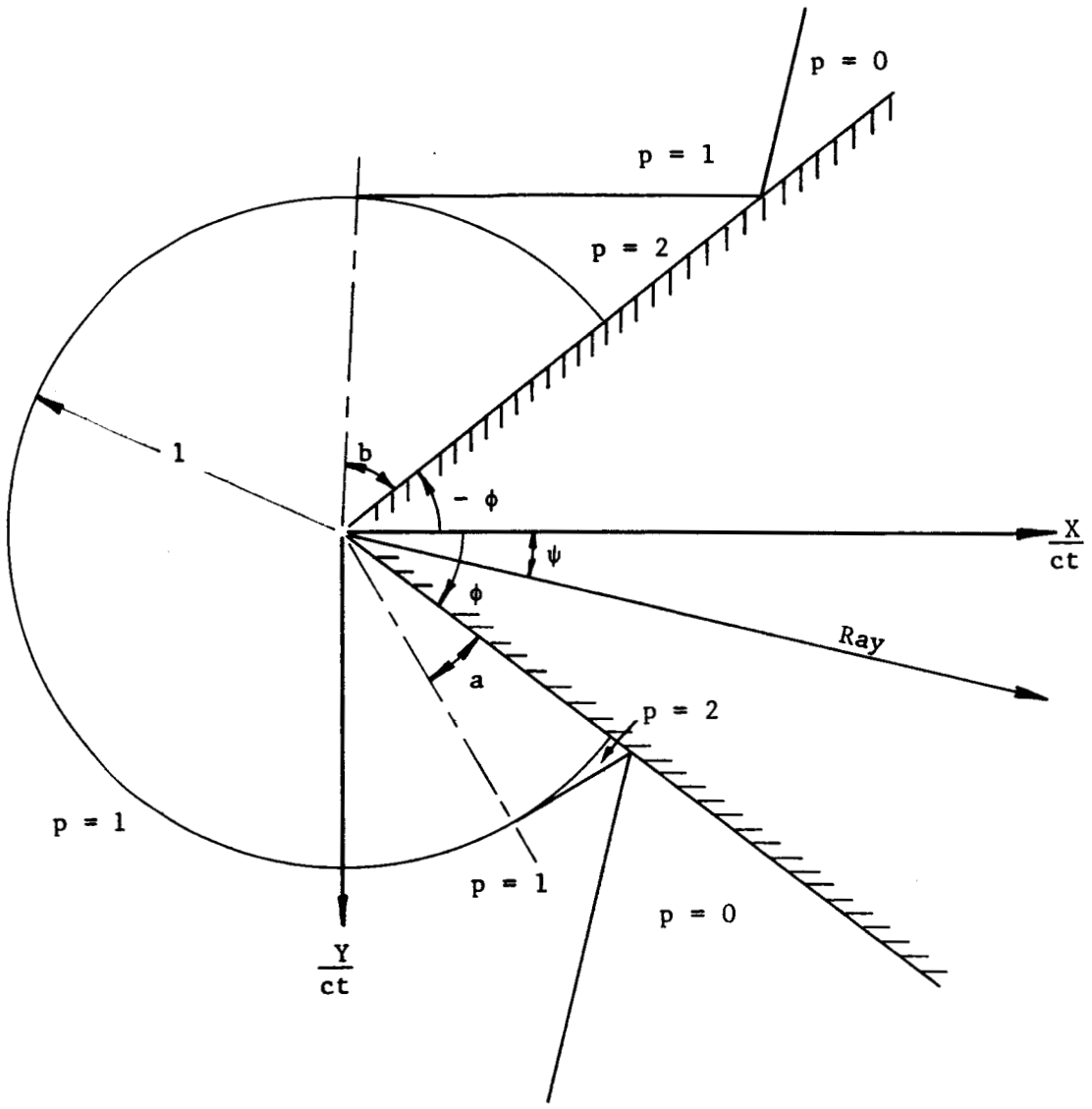

Figure 17 - Diagram of a plane wave intersecting a wedge; Two reflected waves.($\psi < \phi$)

In accordance with the assumption of similarity, $p = p(s, \theta)$. Then (5) becomes:

$$\left[(1-s^2)\, p_s\right]_s + \frac{1}{1-s^2}\, p_{\theta\theta} = 0 \tag{6}$$

If we set

$$\rho \equiv \left(\frac{s-1}{s+1}\right)^{\frac{1}{2}} \tag{7}$$

then (6) becomes LaPlace's equation:

$$\rho\, \frac{\partial}{\partial \rho}\left(\rho\, \frac{\partial p}{\partial \rho}\right) + \frac{\partial^2 p}{\partial \theta^2} = 0 \tag{8}$$

The solution to (8) may be written in the form

$$p = \text{Im } f(Z) \tag{9}$$

where $f(Z)$ is an analytic function of the complex variable $Z = \rho e^{i\theta}$.

Introducing $R = (X^2 + Y^2)^{\frac{1}{2}}$, we have from (4) and (7)

$$Z = \rho e^{i\theta} = \frac{X + iY}{ct + (c^2t^2 - R^2)^{\frac{1}{2}}}$$

$$\rho = \frac{R}{ct + (c^2t^2 - R^2)^{\frac{1}{2}}} \tag{10}$$

The cone $R \leq ct$ is thus mapped into the unit circle $\rho \leq 1$. The problem has been reduced to that of finding the function analytic in an appropriate sector of the unit circle with prescribed imaginary part on the boundary.

The values of p on the boundary of the circle in Figure 16, for $\psi < \phi$, are:

$$p = 0 \text{ on } \rho = 1, \ \phi \leq \theta \leq \phi + a$$

$$p = 1 \text{ on } \rho = 1, \ \phi + a < \theta < 2\pi - \phi - b$$

$$p = 2 \text{ on } \rho = 2, \ 2\pi - \phi - b \leq \theta \leq 2\pi - \phi$$

$$\frac{\partial p}{\partial \theta} = 0 \text{ on } 0 \leq \rho \leq 1, \ \theta = \phi \text{ and } \theta = 2\pi - \phi$$

For Figure 17, where $\psi < \phi$, the boundary values are:

$$p = 2 \text{ on } \rho = 1, \ \phi \leq \theta \leq \phi + a$$

$$p = 1 \text{ on } \rho = 1, \ \phi + a < \theta < 2\pi - \phi - b$$

$$p = 2 \text{ on } \rho = 1, \ 2\pi - \phi - b \leq \theta \leq 2\pi - \phi$$

$$\frac{\partial p}{\partial \theta} = 0 \text{ on } 0 \leq \rho \leq 1, \ \theta = \phi \text{ and } \theta = 2\pi - \phi$$

In order to solve for p, the exterior of the wedge will be mapped from the Z plane onto the upper half of the W plane by the transformation

$$W = \rho_1 e^{iW} = (Ze^{-i\phi})^{\lambda} \tag{11}$$

where $\lambda = \frac{\pi}{2(\pi - \phi)}$

Thus, $\rho = \rho^{\lambda}$, $W = \lambda(\theta - \phi) = \lambda(\theta - \pi) + \frac{1}{2}\pi$. (12)

The circular sector in which p is to be determined becomes a semicircle in the W-plane with $\frac{\partial p}{\partial \theta} = 0$ on the diameter (into which the sides of the wedge transform). By the reflection principle we may extend p into the whole plane, and obtain a boundary value problem in the unit circle; See Figures 18 and 19.

The next step is the determination of a harmonic function p with piecewise constant boundary values. The solution of the problem may be obtained as the

sum of solutions each of which takes on a specified constant value on one arc of the circle and is zero on all other arcs. Suppose $W_2 > W_1$ with $W_2 - W_1 < 2\pi$, and $p = c$ on the arc $W_2 \geq W \geq W_1$ and $p = 0$ elsewhere. Then p can be shown to take the form (Reference 2):

$$p = \frac{c}{\pi}\left[\arg\left\{\frac{W-\exp(iW_2)}{W-\exp(iW_1)}\right\} - \frac{W_2-W_1}{2}\right] \tag{13a}$$

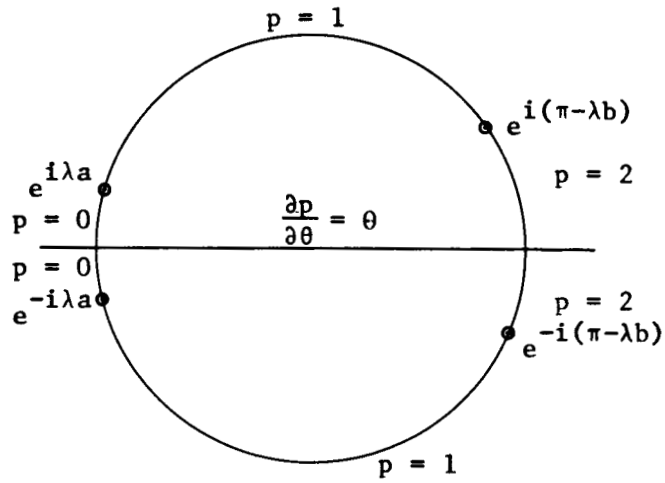

Figure 18 - Complex plane wedge/shock representation.($\psi > \phi$)

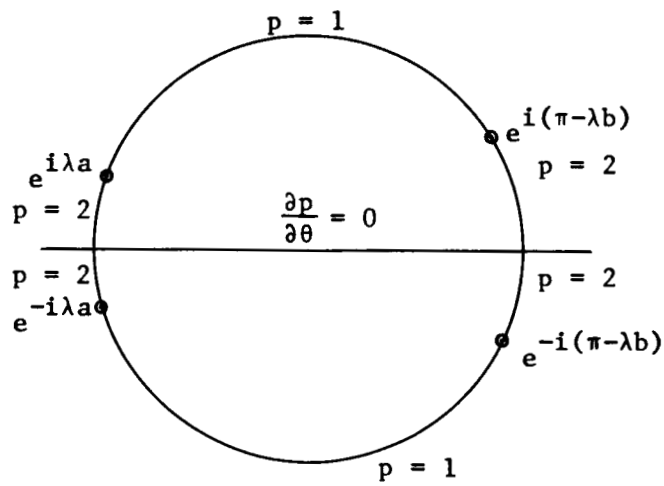

Figure 19 - Complex plane wedge/shock representation.($\psi < \phi$)

And in terms of real variables:

$$p = \frac{c}{\pi} \arctan\left\{ \frac{(1-\rho_1^2)\ \sin\left(\frac{W_2-W_1}{2}\right)}{(1+\rho_1^2)\cos\left(\frac{W_2-W_1}{2}\right) - 2\rho_1 \cos\left(W - \frac{W_2-W_1}{2}\right)} \right\} \tag{13b}$$

The arctangent is taken in the interval between 0 and π. The solutions may then be written explicitly as follows:

Case 1, $\phi \leq \psi \leq \frac{1}{2}\pi - \phi$

$$p = 1 - \frac{1}{\pi} \arctan\left[\frac{-(1-\rho^{2\lambda})\ \cos\lambda\ (\psi-\pi)}{(1+\rho^{2\lambda})\ \sin\lambda\ (\psi-\pi) - 2\rho^{\lambda}\ \sin\lambda\ (\theta-\pi)} \right]$$

$$+ \frac{1}{\pi} \arctan\left[\frac{-(1-\rho^{2\lambda})\ \cos\lambda\ (\psi+\pi)}{(1+\rho^{2\lambda})\ \sin\lambda\ (\psi+\pi) - 2\rho\lambda\ \sin\lambda\ (\theta-\pi)} \right] \tag{14}$$

Case 2, $0 \leq \psi \leq \phi$

$$p = 1 + \frac{1}{\pi} \arctan\left[\frac{(1-\rho^{2\lambda})\ \cos\lambda\ (\psi-\pi)}{(1+\rho^{2\lambda})\ \sin\lambda\ (\psi-\pi) - 2\rho\lambda\ \sin\lambda\ (\theta-\pi)} \right]$$

$$+ \frac{1}{\pi} \arctan\left[\frac{-(1-\rho^{2\lambda})\ \cos\lambda\ (\psi-\pi)}{(1+\rho^{2\lambda})\ \sin\lambda\ (\psi-\pi) - 2\rho\lambda\ \sin\lambda\ (\theta-\pi)} \right] \tag{15}$$

Application to sonic boom incident to a building. - Using equation (14) or (15), one can compute the pressure distribution in a circular arc of radius ct surrounding a corner of a structure struck by a sonic boom wave. The circle defines the region in which the wave is diffracted and reflected due to the presence of the corner. Let:

t = time elapsed since the wave hit the corner of the structure.

H = height of the structure.

Then, if ct>H, the circular sector has reached the ground and has been reflected; the previous formulae cannot be applied directly. Sonic boom waves are always associated with incident bow and tail waves with an expansion region between them (the "N" wave). In addition, both bow and tail waves have ground-reflected waves. The pressure distribution of a sonic boom can be computed as the algebraic sum of the pressure distributions of each of these elements: bow wave (incident and reflected), expansion wave region, and tail wave (incident and reflected). In Figures 20 through 23, a few multiple reflected disturbance regions of a sonic boom wave past a right angled corner are shown. For this case, $\psi=0$, $\phi = \frac{1}{4}\pi$. So equation (15) is to be used to compute the pressure distribution of a diffracted incident wave at point (X_1, Y_1) in the neighborhood of the corner.

Pressure distribution at any time is a function of the height of the point above ground level and the geometry of the reflected disturbance regions.

In the interval $0 \leq ct \leq \sqrt{X_1^2 + Y_1^2}$, $p(X_1, Y_1) = 0$, 1, or 2; the value depends on the wave location at the time.

In the interval $\sqrt{X_1^2 + Y_1^2} < ct \leq \sqrt{X_1^2 + (2H-Y_1)^2}$, (Figure 20), $p(X_1,Y_1)$ can be computed from the equation for disturbance C_1 only. Thus, p_1, the pressure disturbance at p due to C_1, is computed using

$\theta = \arctan(Y_1/X_1) - \phi$, and $R = \sqrt{X_1^2 + Y_1^2}$ and $p = p_1$.

In the interval $\sqrt{X_1^2 + (2H-Y_1)^2} < ct \leq 2H + \sqrt{X_1^2 + Y_1^2}$, (see Figure 21), $p(X_1,Y_1)$ can be computed by treating the point as affected by C_1 and its ground reflected disturbance C_2. C_2 is treated as a mirror image of C_1:

$p_2(X_1,Y_1) = p_1(X_1,2H-Y_1)$.

$p_{2b}(X_1,Y_1)$ is the pressure at the boundary of the region C_2, which may be

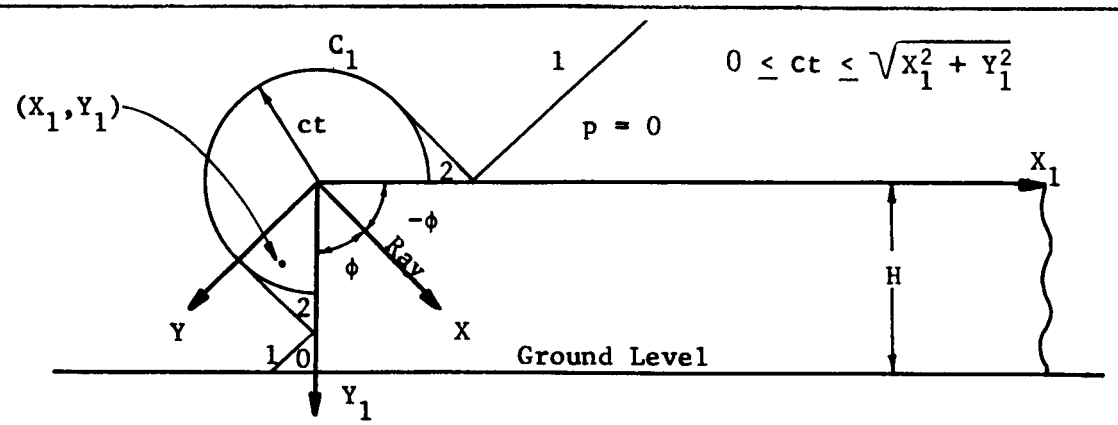

Figure 20 - Wave reflection by a building; Phase I

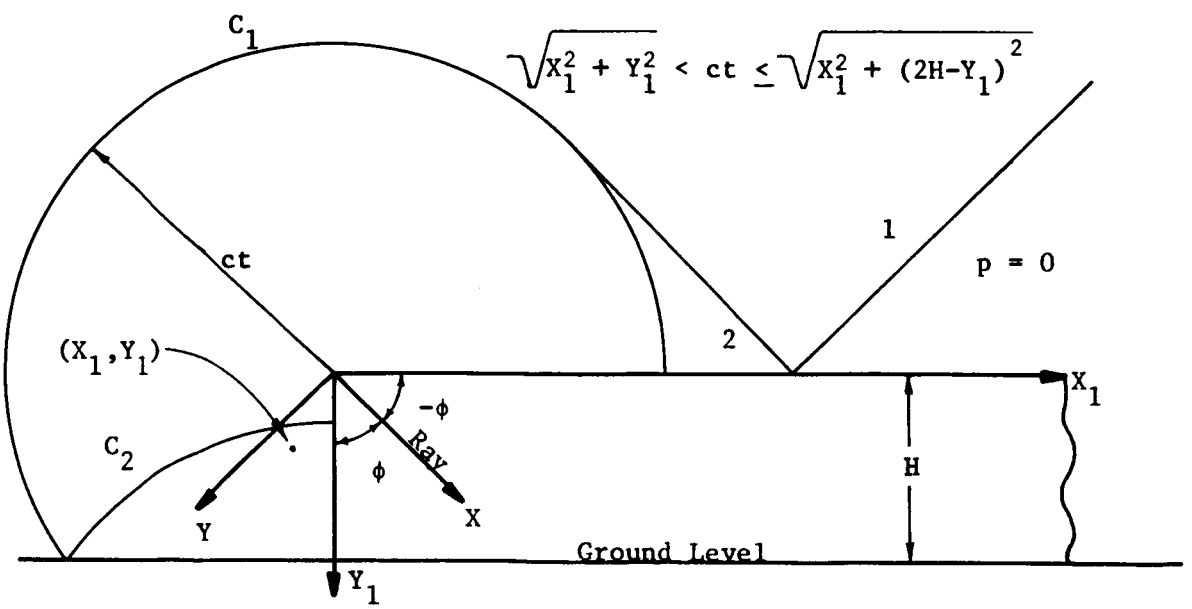

Figure 21 - Wave reflection by a building; Phase II

calculated as the boundary pressure of C_1 with $\theta = \text{arcTan}\left(\frac{2H-Y_1}{X_1}\right) - \phi$.
Then,

$$p(X_1,Y_1) = p_1(X_1,Y_1) + p_2(X_1,Y_1) - p_{2b}(X_1,Y_1) ,$$

where:

for p_1, $R = \sqrt{X_1^2 + Y_1^2}$ and $\theta = \text{arcTan}(Y_1/X_1) - \phi$

for p_2, $R = \sqrt{X_1^2 + (2H-Y_1)^2}$ and $\theta = \text{arcTan}\left(\frac{2H-Y_1}{X_1}\right) - \phi$

for p_{2b}, $R = ct$ and $\theta = \text{arcTan}\left(\frac{2H-Y_1}{X_1}\right) - \phi$

In the interval $\sqrt{X_1^2 + Y_1^2} + 2H < ct \leq 2H + \sqrt{X_1^2 + (2H - Y_1)^2}$ (see Figure 22), $p(X_1,Y_1)$ is affected by the regions of C_1,C_2, and C_3. An exact method would be to compute the boundary values on C_3, assuming that it is affected by regions C_1 and C_2 for $\pi/4 \leq \phi \leq 5\pi/4$ and C_1 only for $5\pi/4 < \phi \leq 7\pi/4$, and then find an exact solution for the pressure at X_1,Y_1 consistent with these boundary

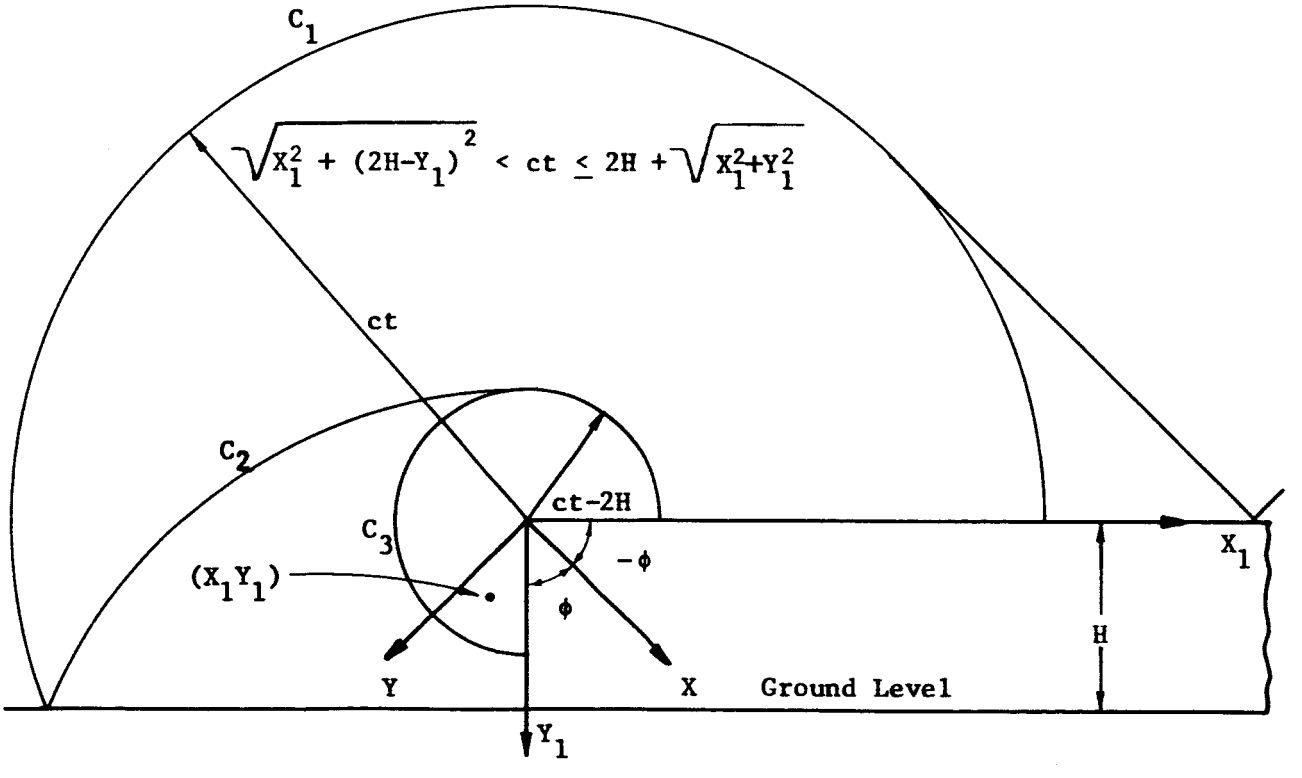

Figure 22 - Wave reflection by a building; Phase III.

conditions. This method is very difficult, if indeed possible, because it requires satisfying variable boundary conditions involving complex expressions. It is therefore suggested that an easier, and perhaps fairly accurate, method is to assume that the influence of region C_3 on the point is due to a peak normal shock of strength equal to the difference of $p_2\ (0,ct-2H)$ and $p_2(0,\sqrt{X_1^2 + Y_1^2})$ at $\phi = 5\pi/4$. Then $p(X_1,Y_1)$ is the sum of the pressures due to C_1,C_2, and C_3:

$$p(X_1,Y_1) = p_1(X_1,Y_1) + p_2(X_1,Y_1) - p_{2b}(X_1,Y_1) + p_2(0,\sqrt{X_1^2+Y_1^2}) - p_2(0,ct-2H)$$

where

for p_1, $R = \sqrt{X_1^2+Y_1^2}$ and $\theta = \arctan(Y_1/X_1) - \phi$

for p_2, $R = \sqrt{X_1^2+(2H-Y_1)^2}$ and $\theta = \arctan\left(\frac{2H-Y_1}{X_1}\right) - \phi$

for p_{2b}, $R = ct$ and $\theta = \arctan\left(\frac{2H-Y_1}{X_1}\right) - \phi$

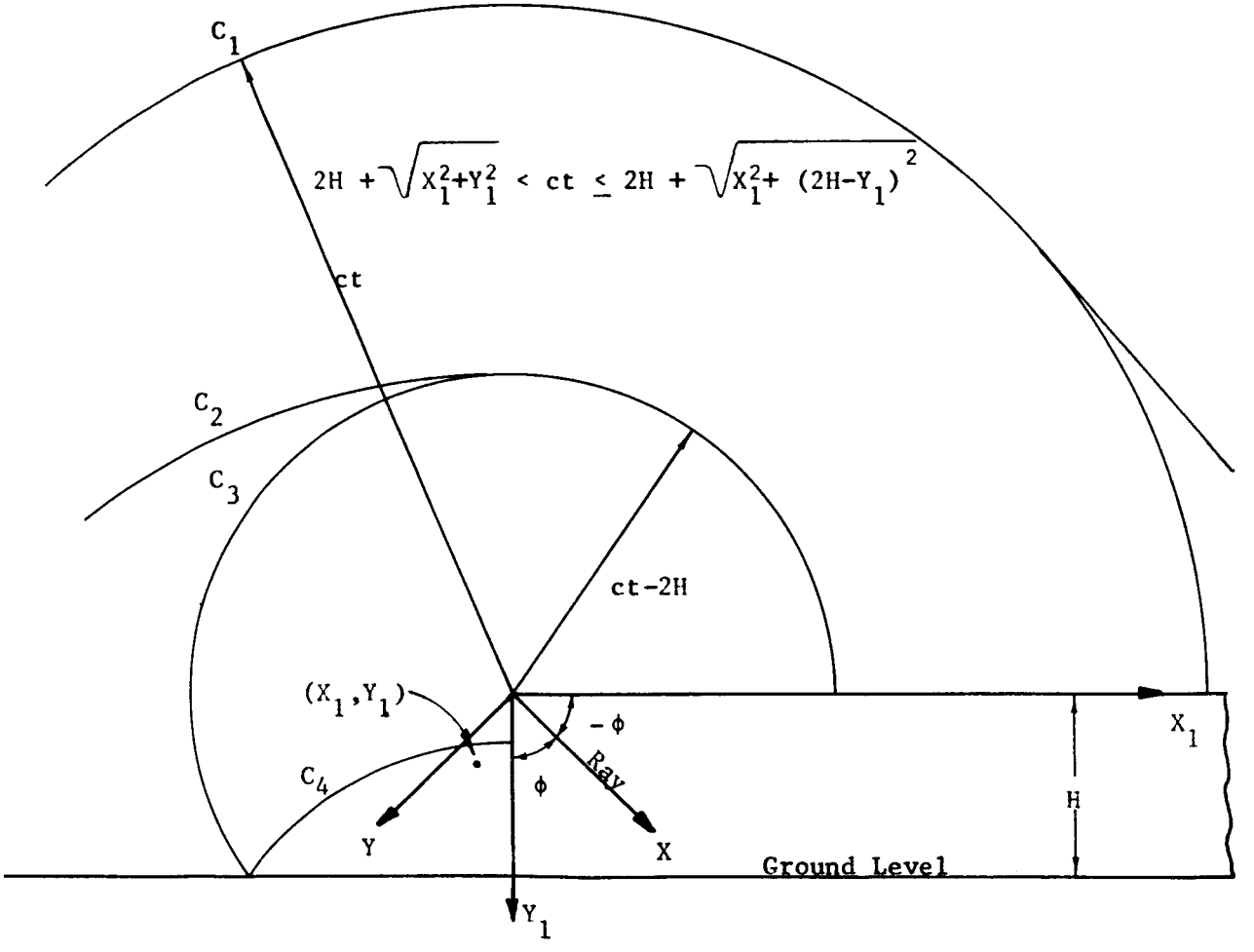

Figure 23 - Wave reflection by a building; Phase IV

for $p_2(0,\sqrt{X_1^2+Y_1^2})$, $R = 2H + \sqrt{X_1^2+Y_1^2}$ and $\theta = \pi$

for $p_2(0,ct-2H)$, $R = ct$ and $\theta = \pi$

In the interval $\sqrt{X_1^2 + (2H-Y_1)^2} + 2H < ct \leq 4H + \sqrt{X_1^2 + Y_1^2}$ (see Figure 23), $p(X_1,Y_1)$ is computed as affected by regions C_1,C_2,C_3, and C_4, with the first three treated as in the previous example. For p_4, C_4 can be considered as the ground reflection of C_3.

By use of a digital computer, this process can be extended to large numbers of reflections and the pressure distributions predicted as functions of time for given wall geometrics and wave incidence angles. Note however, this development applies to two-dimensional cases only, so that the wave must be parallel to the edges of the walls.

Figure 24 depicts the window on the north wall of the Kinney Shoe Store, under the roof overhang, that was broken during the seventh flight of a F-101 aircraft on May 17, 1964. The sonic boom wave for the particular conditions is shown as determined in the previous analysis. For the two-dimensional analysis to consider the corner effects, the wave was assumed parallel to the west wall, neglecting the 3.2° that was estimated in the previous analysis. As shown in Figures 24 to 26, the incident and reflected waves (considering only the bow as a step input at present) are diffracted by the roof overhang and reflected by the ground and roof overhang. The sonic boom wave is considered as a two-dimensional wave and the effects of the north edge of the roof overhang and south-extending west wall are neglected. The wave-history for the window and for some of the points on the north-west corner were estimated using the analysis developed above, considering the effects of the reflected disturbance regions on the rigid walls (the ground and the roof overhang). The X_1 and Y_1 axes were selected as shown in Figure 24. For this particular geometry, $\phi = 0$ and $\psi = 19.9°$. Substituting these values in equation (14),

$$\lambda = \frac{\pi}{2\pi-2\phi} = \frac{1}{2}$$

$$p = 1 - \frac{1}{\pi}\,\text{arcTan}\left[\frac{-(1-\rho)\,\text{Cos}\,\frac{1}{2}(\psi-\pi)}{(1+\rho)\,\text{Sin}\,\frac{1}{2}(\psi-\pi) - 2\rho^{\frac{1}{2}}\,\text{Sin}\,\frac{1}{2}(\theta-\pi)}\right]$$

$$+ \frac{1}{\pi}\,\text{arcTan}\left[\frac{-(1-\rho)\,\text{Cos}\,\frac{1}{2}(\psi-\pi)}{(1+\rho)\,\text{Sin}\,\frac{1}{2}(\psi+\pi) - 2\rho^{\frac{1}{2}}\,\text{Sin}\,\frac{1}{2}(\theta-\pi)}\right] \qquad (16)$$

Simplifying equation (16),

$$p = 1 - \frac{1}{\pi}\,\text{arcTan}\left[\frac{(1-\rho)\,\text{Sin}\,\psi/2}{(1+\rho)\,\text{Cos}\,\psi/2 - 2\rho^{\frac{1}{2}}\,\text{Cos}\,\theta/2}\right]$$

$$+ \frac{1}{\pi}\,\text{arcTan}\left[\frac{(1-\rho)\,\text{Sin}\,\psi/2}{(1+\rho)\,\text{Cos}\,\psi/2 + 2\rho^{\frac{1}{2}}\,\text{Cos}\,\theta/2}\right] \qquad (17)$$

A computer method was developed for the wave history at any point X_1, Y_1 in the coordinate system shown in Figures 24 - 26. The time t = 0 corresponds to the condition at which the incident wave of the sonic boom has reached the origin of the chosen coordinate axes (west edge of the roof overhang). The pressure distribution due to the subject sonic boom was computed at various points on the north wall of the Kinney Shoe Store as in sketch below.

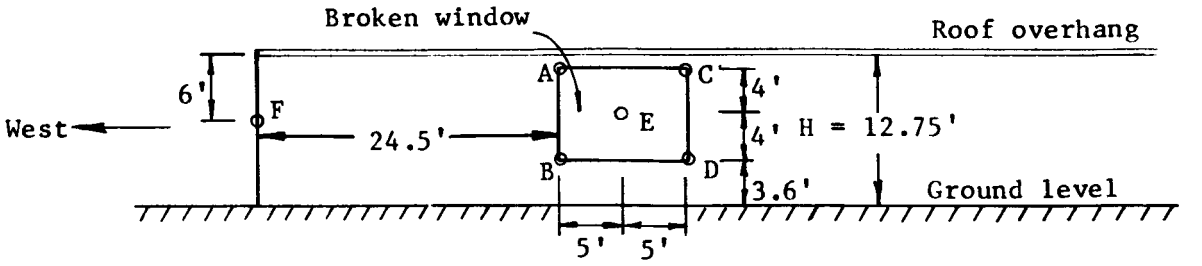

North wall of the Kinney Shoe Store
(view from interior)

In Figure 27, the pressure distribution at points A through F are plotted for a step input wave ($p_i = 0.5$, $p_r = 0.5$).

A sonic boom ordinarily will have the shape of an N-wave. The time interval, Δt, between the bow and tail waves of the sonic boom that caused the broken window has been estimated from related test data to be 0.135 seconds. An N-wave can be treated as two strong shocks of equal strength ($p_i = p_r = \frac{1}{2} \Delta p_o$) and a series of weak expansion waves between them. An N-wave of strength $p_i = 0.5$ and $p_r = 0.5$ at bow and tail waves separated by 0.135 seconds was assumed. Then 135 small expansion waves were assumed of strength $p_i = -1.0/135 = p_r$, each separated by a time interval of 0.001 seconds. A computer program was written and the pressure at any time t_i determined from the sum of the pressures due to all the step waves, effective at that time.

About 15 minutes were required to obtain the pressure history of each point from $t_i = 0$ to $t_i = 0.16$ seconds on an IBM 7040 computer. In Figure 28, the pressure histories of the points A through F are plotted. The dotted lines represent the input wave if there were no corner or overhang effects.

Since the data indicates that Δp_o for the subject flight was about 1.65 psf, multiplication of the points on Figure 28 by 1.65 will give the estimated pressure history on the window exterior.

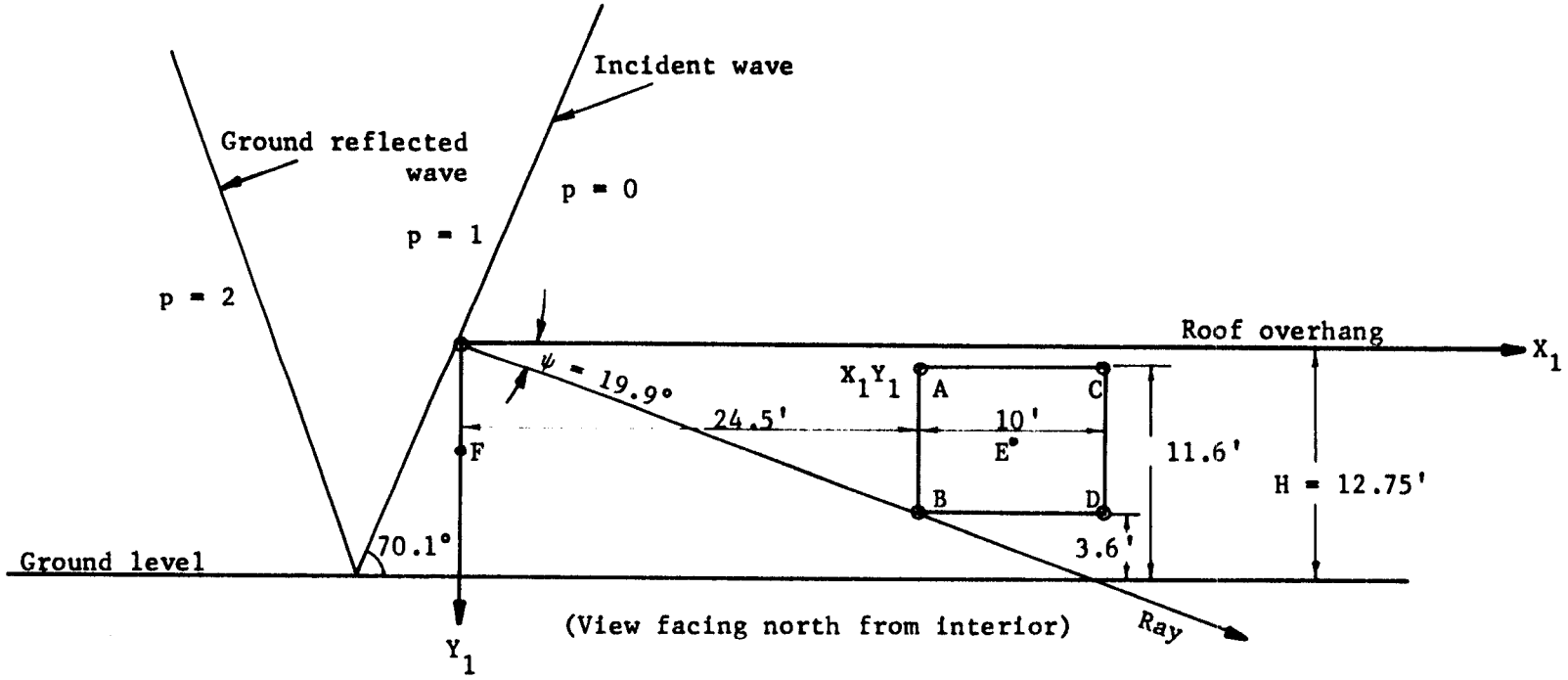

Figure 24 - Geometry of sonic boom and front of Kinney Shoe Store used in the two-dimensional analysis.

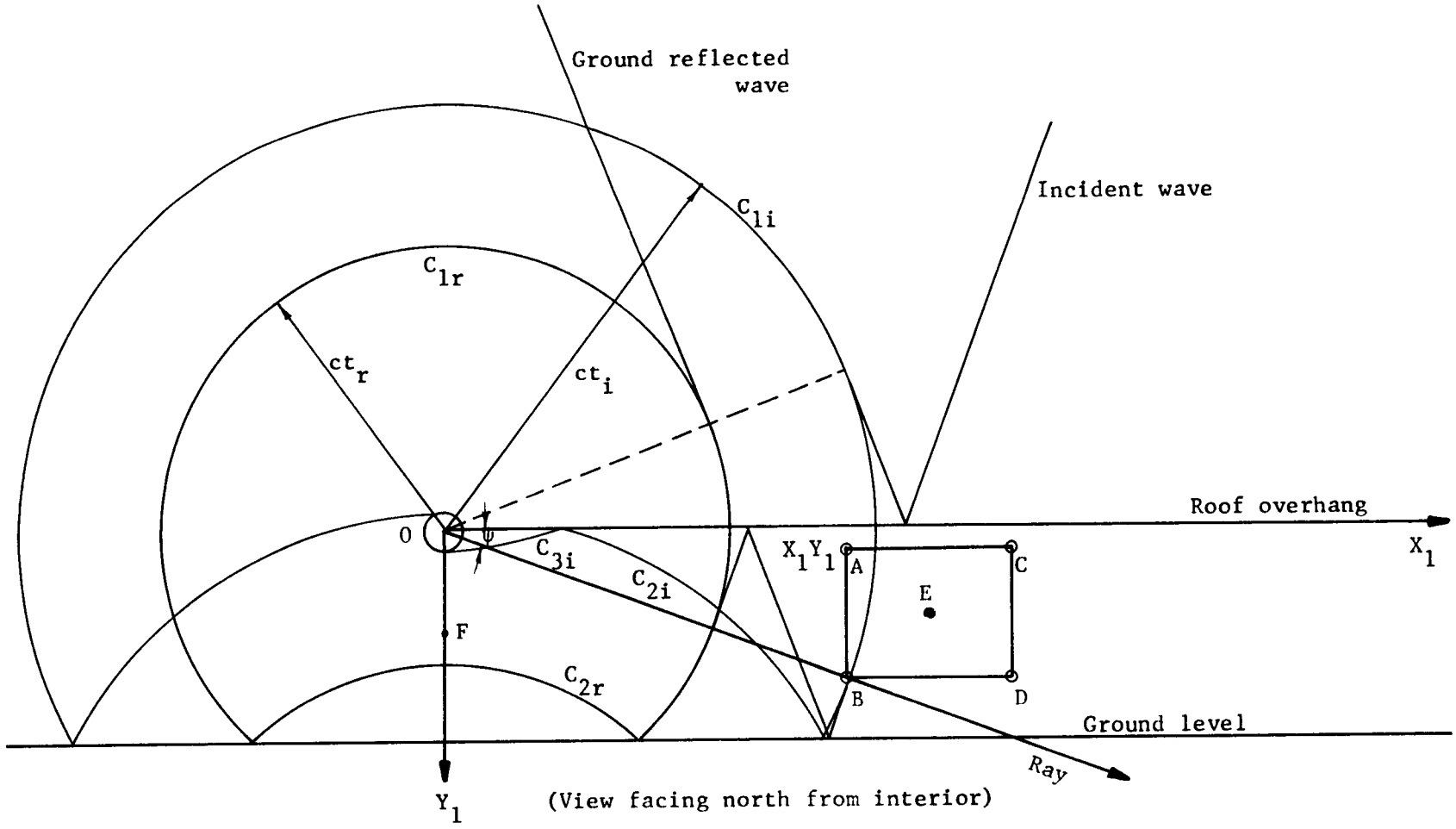

Figure 25 - Incident and reflected wave patterns on the north wall of the Kinney Shoe Store.

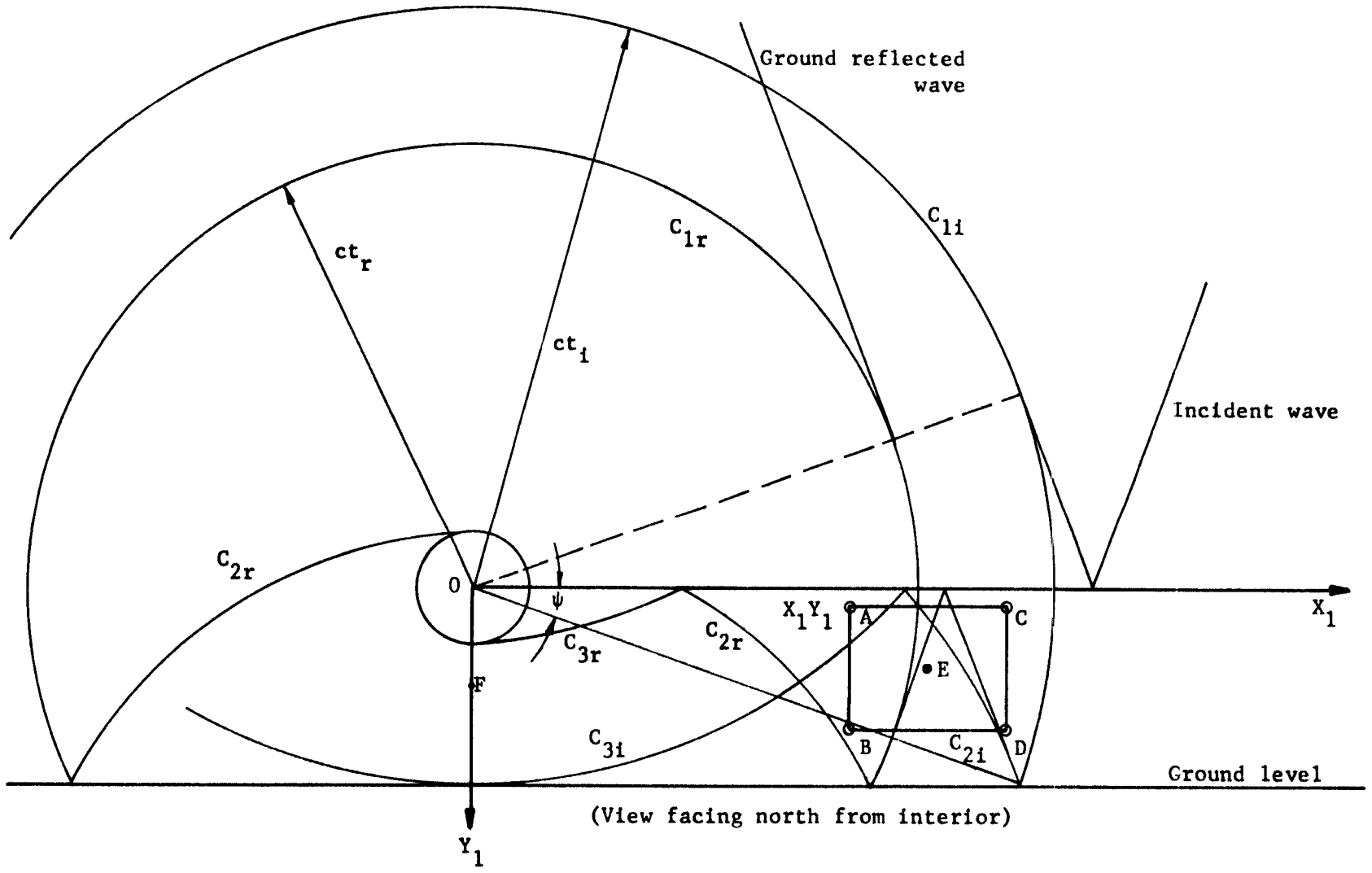

Figure 26 - Incident and reflected wave patterns on the north wall of the Kinney Shoe Store.

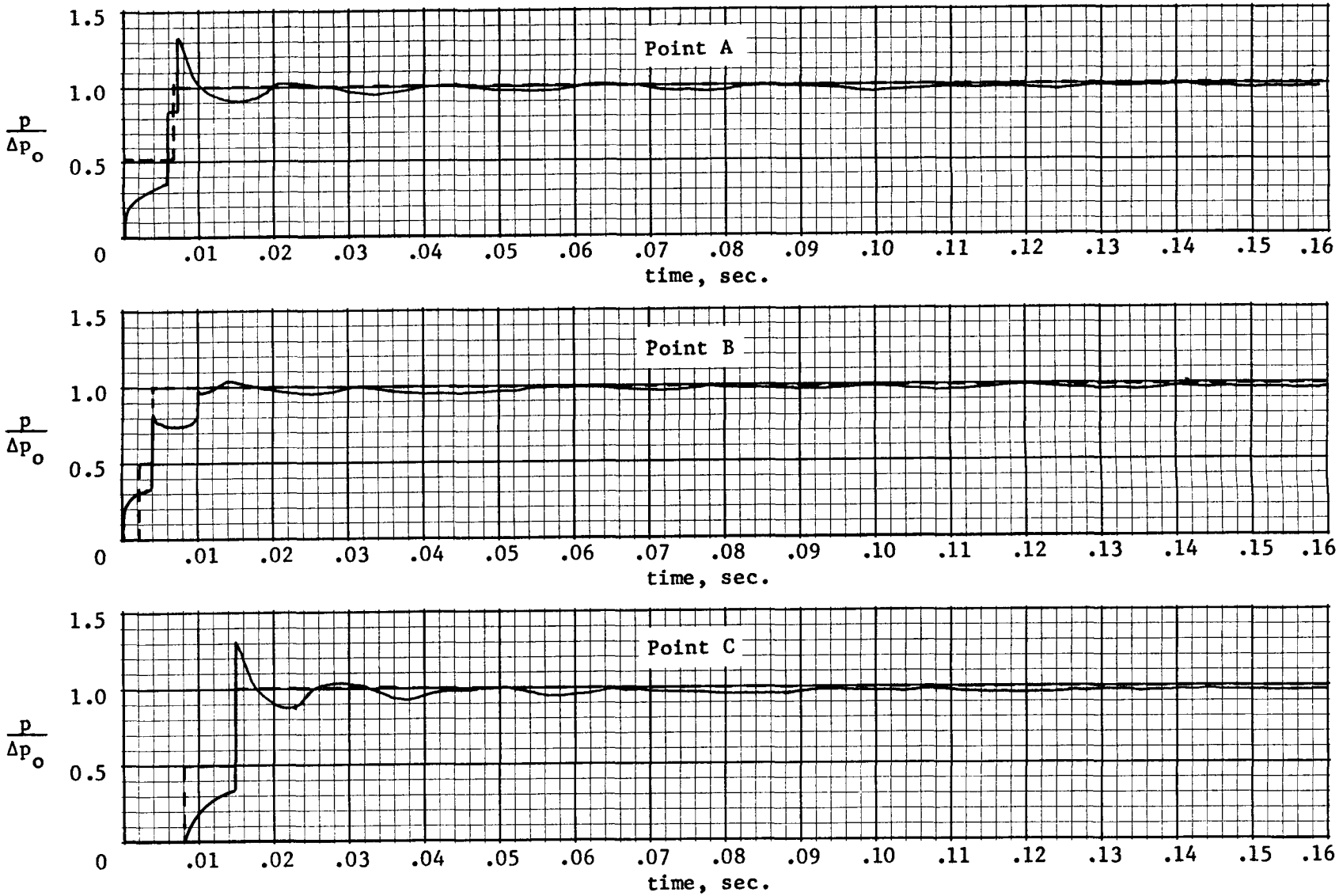

Figure 27 - Computed pressure history at six window points for a step-wave of unit overpressure.

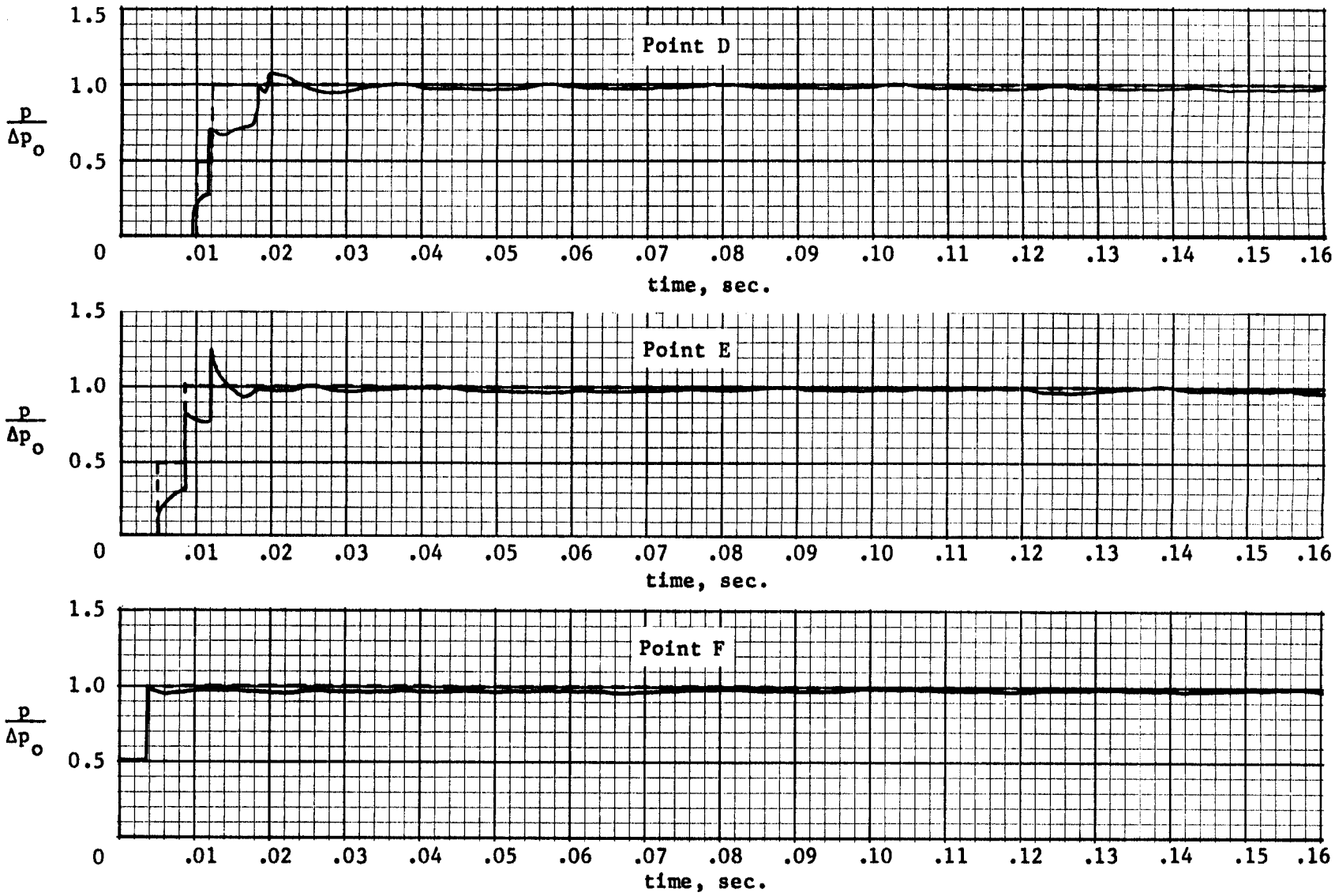

Figure 27 - Concluded.

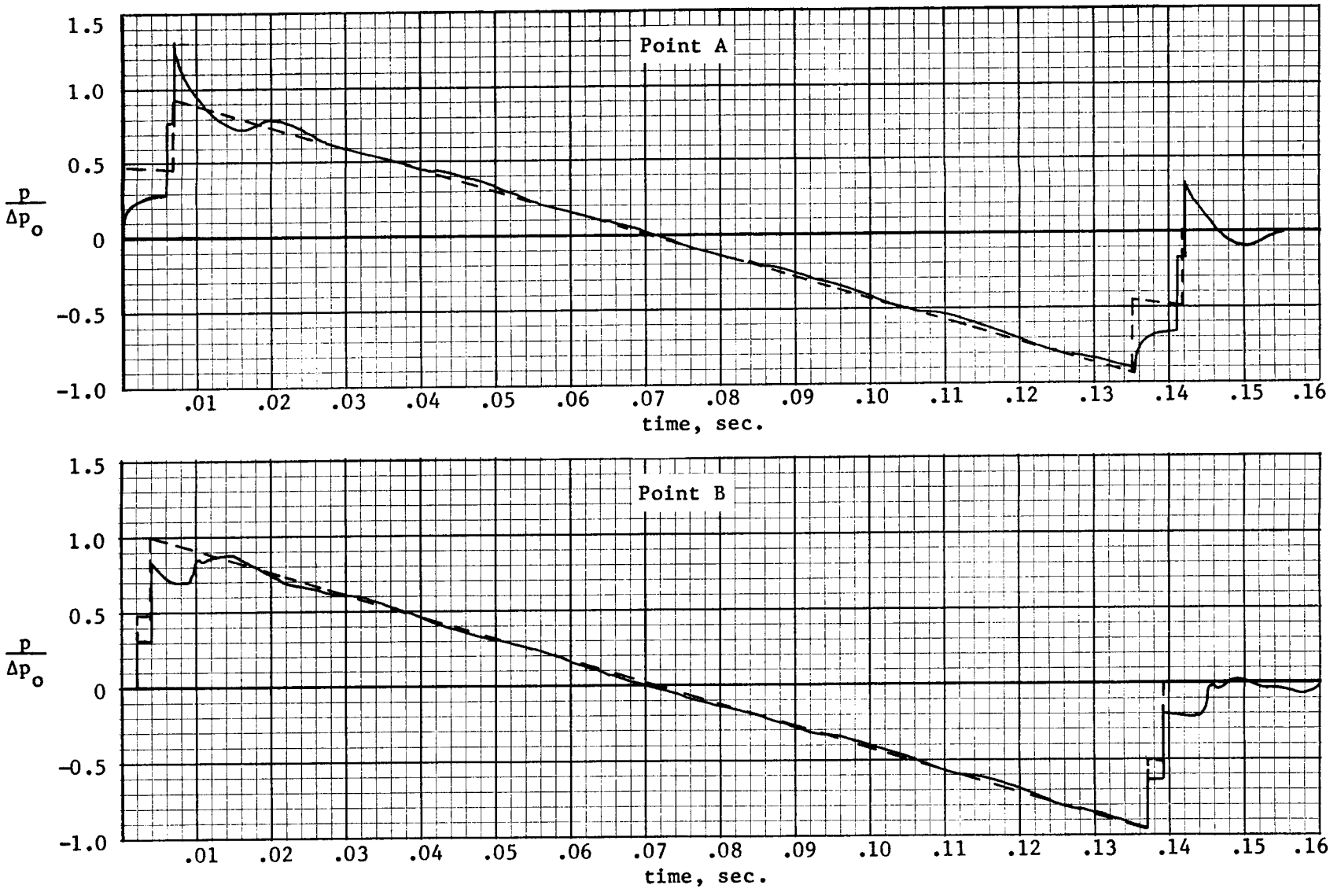

Figure 28 - Computed pressure history at six window points for an N-wave of unit overpressure.

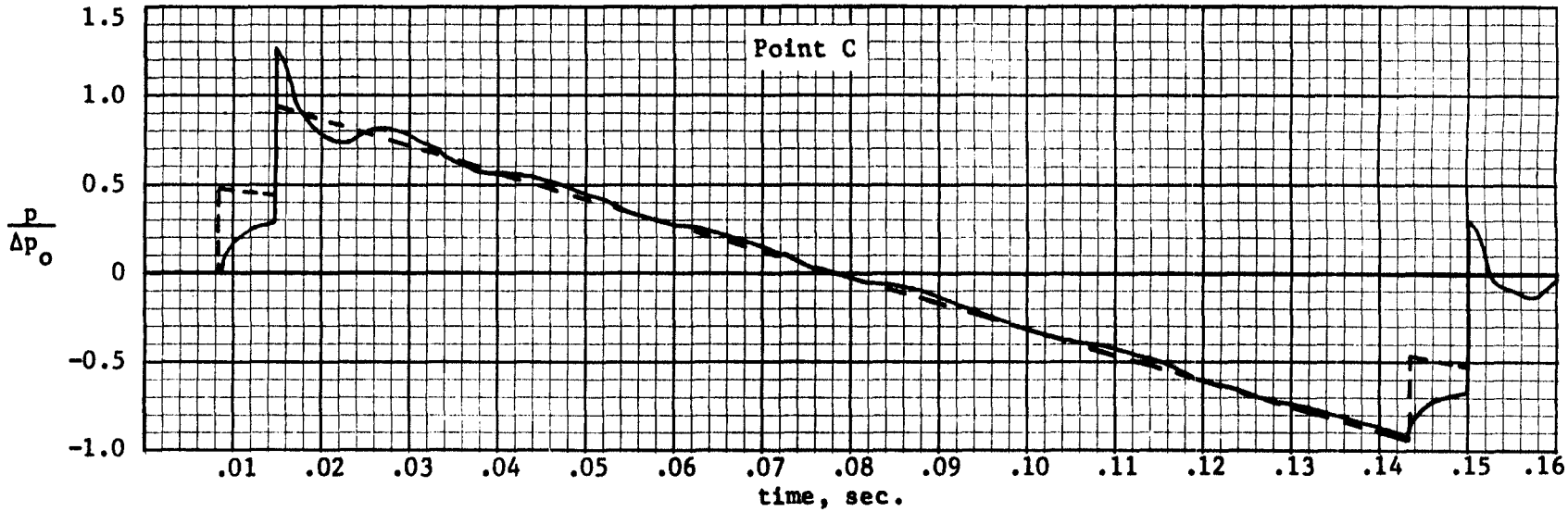

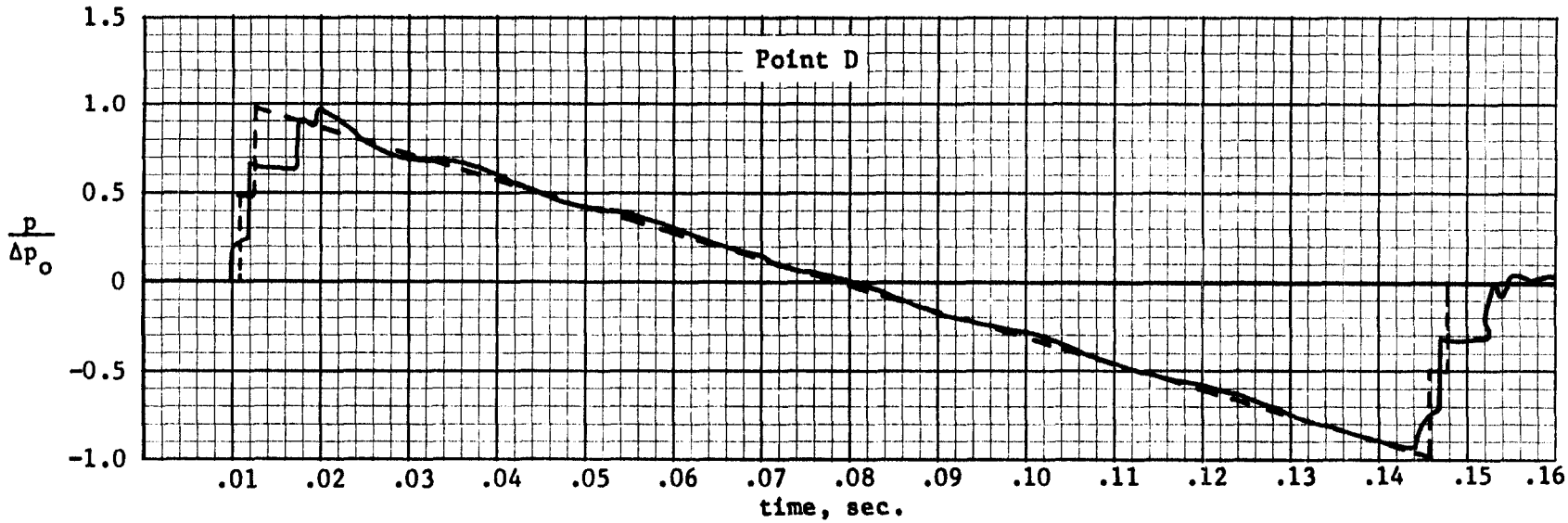

Figure 28 - Continued.

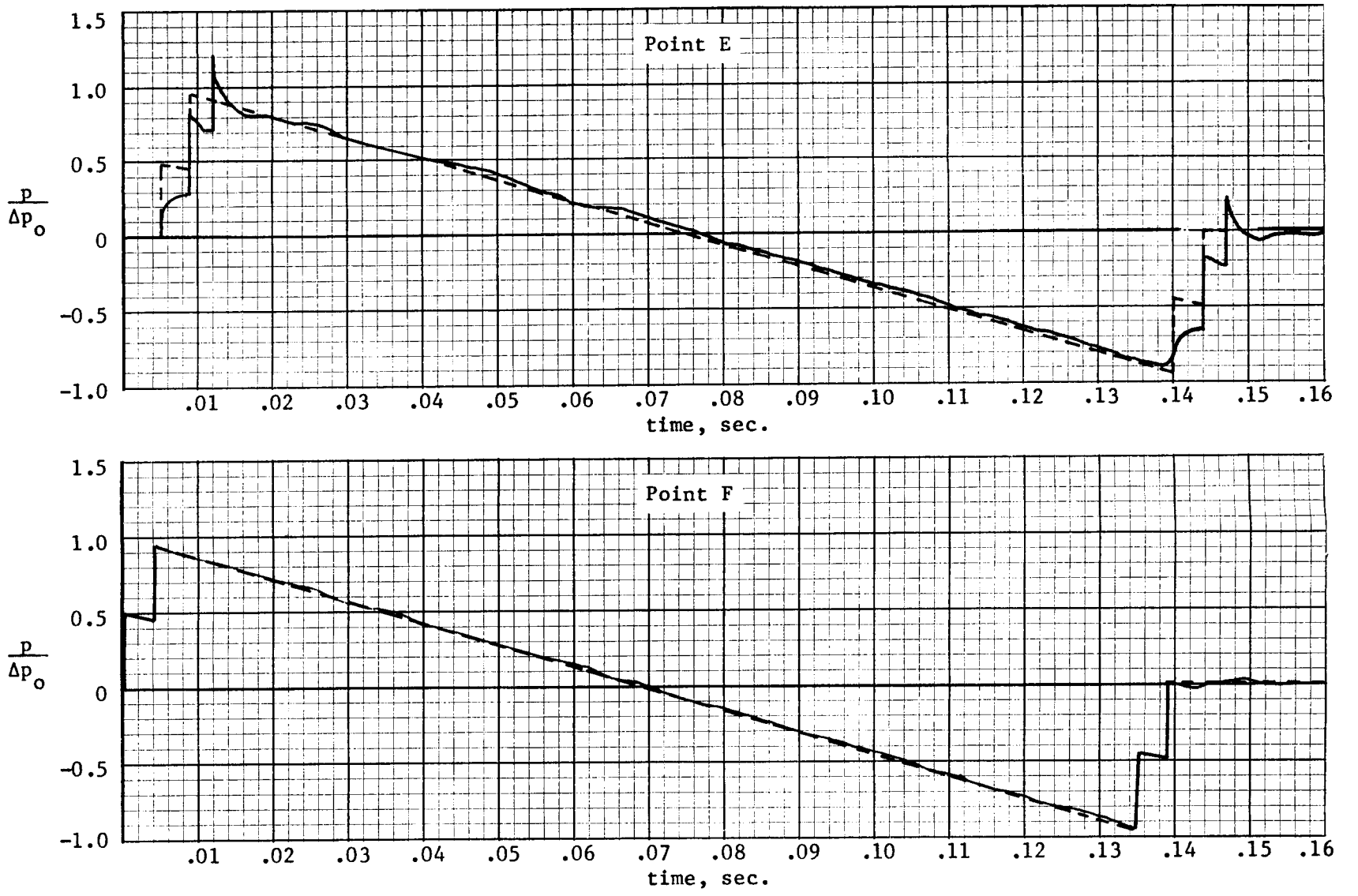

Figure 28 - Concluded.

CONCLUDING REMARKS

The three methods presented for calculating the time-of-passage of an incident wave and the time interval between incident and reflected waves for a wall facing the wave give almost identical results for small offset distances (10,000 feet or less) from the flight track. The differences in results are greatest at low Mach numbers and large offset distances (up to 70,000 feet). The conical wave analysis (Method I) gives the poorest accuracy. The method (Method III) which assumes an atmosphere with a linear variation of acoustic velocity with altitude up to the tropopause and which uses the simplifying assumption of constant ray angle projection in the vertical plane normal to the flight path is considered to be the most practical method.

The method presented and computer method developed for determining the pressure-time histories at the four corner points and mid-point position of the broken window location under the roof overhang of the wall in the "shadow" produced no indication of any abnormal or unusual shock wave acting on this window area. However, the fact that this window did apparently break as a result of the particular flight considered suggests the need for continuing study and investigation in this area.

It is concluded that development of confidence in these or other analytical methods and the determination of the validity of various assumptions as to both atmospheric conditions and flight data values will require specific field tests designed and conducted for this purpose.

Andrews Associates, Inc.
1330 Classen Building
Oklahoma City, Oklahoma, June 20, 1966

REFERENCES

1. Lansing, Donald L.: Application of Acoustic Theory to Prediction of Sonic Boom Ground Patterns from Maneuvering Aircraft. NASA TN D-1860, 1964.

2. Keller, J. B. and Blank, A.: Diffraction and Reflection of Pulses by Wedges and Corners. Communication on Pure and Applied Mathematics, ser. 4, no. 1, June 1951.

3. Luneberg, R. K.: Mathematical Theory of Optics. University of California Press, 1964.

4. Keller, J. B.: Mechanics of Continuous Media. New York University Lectures, 1949-50.